Lappeenranta University of Technology
School of Energy Systems
Degree Program in Energy Technology

Tatu Hovi

MITIGATION OF EXTERNAL PRESSURIZED THERMAL SHOCK IN NUCLEAR REACTOR PRESSURE VESSEL

Examiners: Prof. Juhani Hyvärinen

Supervisors: Research Scientist Jani Laine

TIIVISTELMÄ

Lappeenrannan teknillinen yliopisto
School of Energy Systems
Energiatekniikan koulutusohjelma

Tatu Hovi

Ulkopuolisen paineistetun lämpöshokin lieventäminen ydinreaktorin painesäiliössä

Diplomityö

2017

76 sivua, 45 kuvaa, 10 taulukkoa.

Työn tarkastajat: Professori Juhani Hyvärinen

Hakusanat: PTS, reaktorin painesäiliö, ulkoinen jäähdytys, eristys
Keywords: PTS, reactor pressure vessel, external cooling, insulation

Ydinreaktorin painesäiliön turvallisuus on merkittävä tekijä ydinvoimalaitoksissa, sillä painesäiliö on ainoa komponentti minkä täytyy kestää kaikki mahdolliset onnettomuudet tuhoutumatta. Onnettomuus, mikä voi haastaa painesäiliön kestävyyden tietyissä olosuhteissa, on paineistettu lämpöshokki. Ylijäähtyminen aiheuttaa lämpöshokin, jolloin painesäiliöön kohdistuu suuri lämpötilagradientti. Painevesireaktorin tapauksessa suuri sisäinen paine yhdessä lämpötilagradientin kanssa voi murtaa painesäiliön seinämän, jos painesäiliössä on valmiita haurasmurtumia. Tässä työssä keskitytään ulkopuolisen lämpöshokin tutkimiseen ja sen lieventämiseen käyttäen lämpöeristeitä. Tavoitteen saavuttamiseksi työssä käytetään numeerista mallia, mikä pystyy arvioimaan lämmön siirtymistä ja lämpötilojen jakaumia reaktorin painesäiliön seinämässä sekä lämpöeristeissä. Lämpöjakaumia voidaan käyttää painesäiliön kestävyyden määrittämisessä.

ABSTRACT

Lappeenranta University of Technology
School of Energy Systems
Degree Program in Energy Technology

Tatu Hovi

Mitigation of external pressurized thermal shock in nuclear reactor pressure vessel

Master's Thesis

2017

76 pages, 45 figures, 10 tables
Examiners: Prof. Juhani Hyvärinen

Keywords: PTS, reactor pressure vessel, external cooling, insulation

The safety of reactor pressure vessel in nuclear power plant is significant because the reactor pressure vessel is the one component that has to withstand all the possible accident scenarios without failing. One accident scenario that challenges the reactor pressure vessel integrity under specific conditions is pressurized thermal shock. Overcooling causes thermal shock where large temperature gradient has an impact on the reactor pressure vessel. In the case of pressurized water reactor, the internal pressure together with temperature gradient can lead to fracture of the reactor pressure vessel if there are existing defects within the reactor pressure vessel. This work is focused on researching the impact of external pressurized thermal shock on the reactor pressure vessel. The goal is to investigate the mitigation of pressurized thermal shock by thermal insulation. For achieving the goal, this work utilizes a script that is capable of calculating heat transfer and temperature distributions within the reactor pressure vessel and thermal insulation. Temperature distributions can be used to estimate the integrity of the reactor pressure vessel.

ACKNOWLEDGEMENTS

I want to express my deepest gratitude to Professor Juhani Hyvärinen and Timo Toppila for the guidance, feedback and for providing the opportunity to do this thesis. I also want to thank Sampsa Launiainen and my supervisor Jani Laine for their contributions during writing of this thesis. I am very grateful for my family and friends for their support. Finally, I want to give hearty thank you to my girlfriend Yoo Yeon for the continuous loving support during the writing of this thesis.

TABLE OF CONTENTS

1 INTRODUCTION 5

1.1 BACKGROUND OF THE THESIS 5

1.2 GOALS AND DELIMITATIONS 6

1.3 STRUCTURE OF THESIS 6

2 PRESSURIZED THERMAL SHOCK 8

2.1 PTS ANALYSIS PROCEDURE 9

2.2 PTS IN LOVIISA NPP 11

2.2.1 Loviisa RPV 11

2.3 POSTULATED RAPID COOLING OF THE EXTERNAL SIDE OF RPV 13

2.3.1 Conditions and transient progression 15

2.4 REDUCTION OF PTS 18

2.4.1 General methods 18

2.4.2 Thermal insulation of sensitive weld 19

3 THERMAL INSULATION 20

3.1 REQUIREMENTS FOR INSULATION MATERIAL 20

3.1.1 Thermal conductivity 21

3.1.2 Thermal diffusivity 22

3.1.3 Temperature resistance 23

3.1.4 Radiation resistance 24

3.1.5 Versatility and durability 25

3.1.6 Corrosion effect 25

3.1.7 Optimization of thermal insulation thickness 25

3.2 THERMAL INSULATION METHODS 26

3.3 ATTACHMENT 26

3.4 REJECTED INSULATION MATERIALS 26

3.5 POTENTIAL INSULATION MATERIALS 27

3.5.1 MACOR™ 27

3.5.2 Calcium silicate 27

3.5.3 Stainless steel AISI316 29

3.5.4 Titanium Ti-6Al-4V 29

3.5.5 Zirconium 30

4 TEMPERATURE DISTRIBUTION ANALYSIS 31

4.1 ASSUMPTIONS 31

4.1.1 Vertical plate *32*
4.1.2 Transient progression in calculations *32*
4.1.3 Contact resistance *34*
4.2 CORRELATIONS 34
4.3 MATLAB SCRIPT 37
4.4 MATLAB SCRIPT VALIDATION 41
4.4.1 Validation by FLUENT simulation *41*
4.4.2 Validation by experimental data *43*
4.5 TEST FACILITY IN LUT 46
5 TEMPERATURE DISTRIBUTION RESULTS 49
5.1 RPV WITHOUT THERMAL INSULATION 50
5.2 MACOR 52
5.3 CALCIUM SILICATE 55
5.4 STAINLESS STEEL AISI316 57
5.5 TITANIUM TI-6AL-4V 59
5.6 ZIRCONIUM 62
5.7 STEADY STATE DISTRIBUTIONS 64
6 CONCLUSIONS AND FURTHER RESEARCH 67
REFERENCES 70

NOMENCLATURE

Latin letters

c_p	specific heat capacity	J/kgK
D	diameter	m
F	convective boiling factor	-
g	gravitational acceleration	m/s^2
h	heat transfer coefficient	W/m^2K
k	thermal conductivity	W/mK
L	characteristic length	m
$\dot{m}$	mass flow rate	kg/s
N	node number	-
n	location nominator	-
p	pressure	Pa, bar, atm
q	heat flux	W/m^2
R	unit thermal resistance	m^2K/W
S	nucleate boiling suppression factor	-
T	temperature	K, °C
t	time	s
x	distance	m
X	local vapour quality	-
X_{tt}	Lockhart-Martinelli parameter	-

Greek letters

α	thermal diffusivity	m^2/s
β	thermal expansion coefficient	K^{-1}
μ	viscosity	Pa s
ν	kinematic viscosity	m^2/s
ρ	density	kg/m^3
σ	surface tension	N/m

Subscripts

cc	Churchill-Chu

db	Dittus-Boelter
fz	Foster-Zuber
H	hydraulic
L	liquid
LV	liquid-vapour
s	surface
sat	saturation
tp	two-phase
V	vapour
w	wall
∞	coolant

Abbreviations

CHF	Critical Heat Flux
ECCS	Emergency Core Cooling System
FEM	Finite Element Method
IAEA	International Atomic Energy Agency
LUT	Lappeenranta University of Technology
NDT	Nil-Ductility Temperature
NPP	Nuclear Power Plant
PIV	Particle Image Velocimetry
PRA	Probabilistic Risk Assessment
PTS	Pressurized Thermal Shock
RPV	Reactor Pressure Vessel

Dimensionless numbers

Bi	Biot number
Fo	Fourier number
Gr	Grashof number
Ra	Rayleigh number
Re	Reynolds number

1 INTRODUCTION

1.1 Background of the thesis

Safety systems and important components in nuclear power plants (NPP) are designed to give immense amount of security during accident scenarios. It is important to have the safety systems and important components in top conditions since they are subjected to various range of ageing mechanisms. To keep these systems and components operational and in reliable working condition, they are regularly inspected, repaired and replaced. The component that is impossible or economically unviable to replace is the reactor pressure vessel (RPV). The safety significance of the RPV is that it is the one component in NPP which cannot be allowed to fail under any circumstances, because the consequences would be impossible to mitigate effectively. Thus the integrity of RPV can potentially define the NPP life-limiting conditions. To increase the credibility of RPV integrity, there are higher margins in load bearing capacity that occur during the operation of NPP. However the RPV material properties are under slow degradation by neutron irradiation, thermal ageing and other ageing mechanisms. [1]

Neutron irradiation from reactor core causes very slowly material embrittlement within the RPV. Embrittled material has lost some of its ductility and experienced increase in ductile-to-brittle transition temperature. This temperature is also known as nil ductility temperature (NDT). When material temperature is below NDT it can fracture easily when deformed. Under normal NPP conditions this will not be a significant risk since the coolant temperature in primary loop is always higher than the NDT of the RPV. [2]

In Loviisa NPP, accident scenarios have been mapped out where sudden cooling of the RPV can occur and the temperatures could fall below the NDT level. Typically these kind of thermal shock accident scenarios are caused by rapid cooling on the internal side of the RPV, but there are also rarer cases where the external side experiences the similar thermal shock. Even though these accident scenarios are very unlikely to happen, a deep understanding of these accidents are important for increasing the safety of the RPV.

1.2 Goals and delimitations

The purpose of this thesis is to study specifically the impact of external thermal shock on the Loviisa NPP RPV and investigate mitigation of thermal stresses by external thermal insulation. Thermal shocks are difficult phenomenon and acquiring a deep understanding of thermal shocks typically requires real experiments. Heat transfer experiments on external thermal shock have been researched in Lappeenranta University of Technology (LUT) by using heat transfer test facility that is located in the University. However in this study the real experiments were not performed and therefore the study of external insulation is limited to methods that can be calculated and simulated rather easily.

The goal is to identify the necessary requirements for thermal insulation materials so they can withstand the challenging conditions around the Loviisa RPV. The defined requirements can further be used in the future if more research and development is performed. Another goal of this thesis is to develop script capable of calculating temperature field distributions within RPV and the thermal insulation during rapid transient cooling. These temperature distribution results can be used as input data for RPV integrity calculations. The final decision in the regard of using the external thermal insulation is up to the owner of Loviisa NPP.

1.3 Structure of thesis

The chapter 2 introduces some background information about pressurized thermal shock (PTS), and briefly clarifies how and why PTS analyses are generally done in NPP. Chapter also includes more specific information about postulated external thermal shock in Loviisa NPP and the general ways of mitigation.

The third chapter is about thermal insulation that is proposed as one potential solution for mitigating the thermal shock. The requirements for potential insulation materials are introduced, along with some passed materials and rejected materials. The challenge in attaching the thermal insulation and other possible thermal insulation methods are also

included in this chapter.

The fourth chapter introduces temperature distribution analysis. The assumptions, boundary conditions, correlations, developed Matlab script and the validation of the script are found in this chapter. A brief review of current state of the heat transfer test facility located in LUT is included in the end of the chapter. The following chapter displays the results from the simulations of external thermal shock, including RPV with and without thermal insulation and steady state calculations for few selected cases. Finally the conclusions and further research suggestions are discussed.

2 PRESSURIZED THERMAL SHOCK

Material experiences a thermal shock when it is rapidly cooled down. The rapid temperature drop makes the material to contract due to thermal expansion and this causes thermal stresses within the material. In NPPs the event of rapid cooling in RPV is defined as pressurized thermal shock because the rapid cooling is often paired with higher internal pressure. PTS only by itself is not significant risk to the RPV; however the PTS under very specific conditions can challenge the RPV integrity.

The RPV is exposed to neutron radiations that are slowly resulting in localized embrittlement of RPV steel and weld materials. The risk is possible if RPV has defects of critical sizes due to embrittlement and if severe transients within NPP system were to occur it could have destructive impact by propagating defects rapidly through the vessel ultimately leading to fracture or even the destruction of RPV. Normally the defects of critical sizes are very unlikely to happen due to regular inspection of RPV integrity. The severe transients that can lead to RPV fracture are called PTS events. PTS events are divided into internal and external cooling of the RPV surface. PTS events also typically involve repressurization of the RPV. Combination of both under specific conditions gives a challenge to the integrity demands for RPV. [3, 4]

Probabilistic risk assessment (PRA) and engineering judgment has successfully identified various scenarios leading to PTS. Typical scenarios include loss of coolant accidents (LOCA), large secondary leaks, stuck open pressurizer safety or relief valve, primary to secondary leakage accidents, inadvertent actuation of high pressure injection or make-up systems and accident scenarios resulting in cooling of RPV from external side. When a scenario such as LOCA happens in primary system, the water level may drop rapidly. NPP operators and automatic systems provide reserve water in order to prevent overheating in the core. Provided water is generally much colder than the water in primary system. The combination of temperature drop and repressurization causes significant thermal stresses on the RPV wall that could potentially initiate propagation of existing defects. [1, 3]

Fortunately, the chances that defects of critical sizes exist in the embrittled RPV and weld material with the combination of severe PTS are very low probability event. The subtlety in nuclear safety is that even the most unlikely accident scenarios are assumed to happen

and that leads to the research and development which is making the nuclear energy more secure.

2.1 PTS Analysis procedure

The PTS analysis procedure is performed as series of sequential steps as shown in the flowchart in Figure 1. The procedure starts with selecting and defining the PTS sequence. [1]

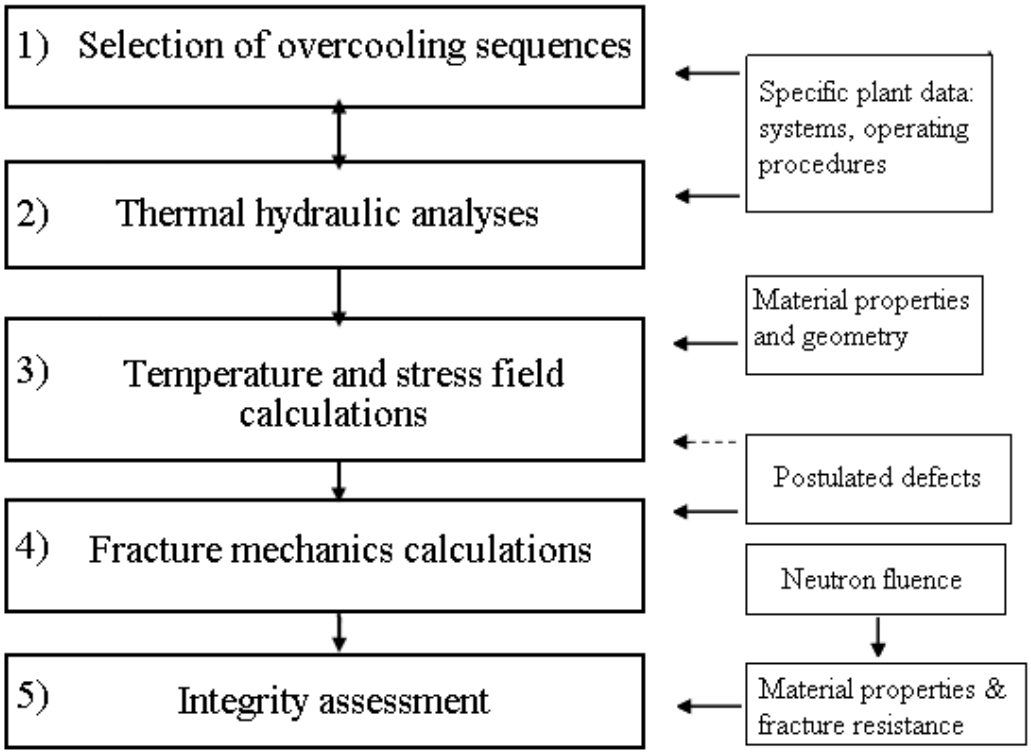

Figure 1. PTS analysis flowchart.

The selection of PTS transients (Figure 1, 1) is often based on identified accident scenarios in the safety analysis reports. The main goal is to identify accident scenarios that are direct PTS events themselves or are accidents with other consequences that can lead to PTS event. Different sequences in PTS analysis are frequently unit specific. Depending on the unit, all the relevant, meaningful and unique plant features are taken into consideration. Typically some of the sequences are defined in terms of severity where PRA has been

used. Comprehensive probabilistic PTS studies are used to select the most important PTS sequences contributing to RPV failure risk. [1, 4]

Thermal hydraulic analyses (Figure 1, 2) are used to assist the transient selection process and to provide some necessary input data for analyzing RPV structural integrity. Analysis is typically done by specific thermal hydraulic code or combination of codes. The following parameters are provided by thermal hydraulic analyses:

- Fluid temperature field in downcomer or external side of the RPV.
- Primary circuit pressure.
- Local heat transfer coefficients of wall-to-coolant.

Coolant temperature field and local heat transfer coefficients are replaced with inner surface temperatures of the RPV wall if the thermal hydraulic code is able to provide it. [1, 4]

Temperature and stress field calculations (Figure 1, 3) in the RPV wall during PTS transients are crucial for determining the integrity of the vessel. Calculations for stress fields are required for each time steps. Stresses are typically solved by numerical or analytical methods. Analytical methods are more used in specific justified cases. Solving stress fields by using the finite element method (FEM) is used in most cases. [4]

Fracture mechanics calculations (Figure 1, 4) are part of structural analysis. In structural analysis the aim is to evaluate stress intensity factors for postulated defects within the RPV that are under tension by thermal hydraulic transients. Fracture mechanics are based on static fracture toughness and they are used to estimate brittle failure in the RPV with postulated defects. In most defects and transient combinations the linear elastic fracture mechanics is sufficient approach, where the intensity factor K_I is acceptable. The values for intensity factor K_I are typically solved by numerical methods based on FEM where the postulated defects are included in the meshed geometry. [1, 4]

Integrity assessment (Figure 1, 5) is the final stage in the evaluation of PTS analysis. It includes evaluation of final results, safety factors and assessment of uncertainties in the results. [1, 4]

2.2 PTS in Loviisa NPP

PTS transient scenarios have been widely researched for Loviisa NPP units one and two. Most of the relevant PTS sequences are internal and few are external. In Loviisa, the main factors that influenced the most in the selection of overcooling sequence for PTS analysis procedure were:

- The probability of accident occurrence.
- Occurrence of cold plumes in the downcomer
- Repressurization of primary circuit.
- The rate at which primary circuit is cooled down.
- The final temperature of primary circuit.

Typical feature for PTS-analysis is that the conservative assumptions are usually the opposite when comparing to traditional safety analysis procedures in NPP. Considering the PTS in RPV, the situation is more severe when emergency core cooling system (ECCS) is working as planned and the injected ECCS water is as cold as possible. [5] The thermal hydraulic analyses in Loviisa have been completed by using APROS [6] simulation program supported with REMIX [7] thermal mixing simulations for cold plume scenarios.

2.2.1 Loviisa RPV

The purpose of RPV is to contain the reactor core, core shroud and the coolant. RPV is one of the most important components in NPP since it is practically irreplaceable and it has to withstand high temperature, pressure and neutron irradiation throughout NPP's operational lifetime. It is also crucial for RPV to be able to withstand all relevant postulated accident scenarios.

LO1 and LO2 have almost identical RPV structure. Both RPVs were manufactured in Soviet Union and they consist of seven circular shells that are welded together. Both have the thickness of 140mm for RPV shell. The internal side of RPV has three-layered cladding for corrosion protection. The cladding has a thickness of 9-10mm. The exceptions in thicknesses are in the location of welds number 6 and 7, where the thickness is 205mm

without including cladding. Base materials for both RPVs are quenched and tempered low alloyed chrome-molybdenum-vanadium steel. [8, 9] Table 1 contains properties of base and weld materials of LO2 RPV in different temperatures. The rolled out overview of LO2 RPV and weld locations (right side in the figure) are presented in Figure 2.

Table 1. Base and weld material properties of LO2 RPV. [10]

Parameter		**Unit**	**Temperature** [°C]			
			20	100	200	300
Thermal conductivity,	k	[W/mK]	40.2	39.8	38.8	37.9
Specific heat capacity,	c_p	[J/kgK]	502			
Density,	ρ	[kg/m^3]	7800			

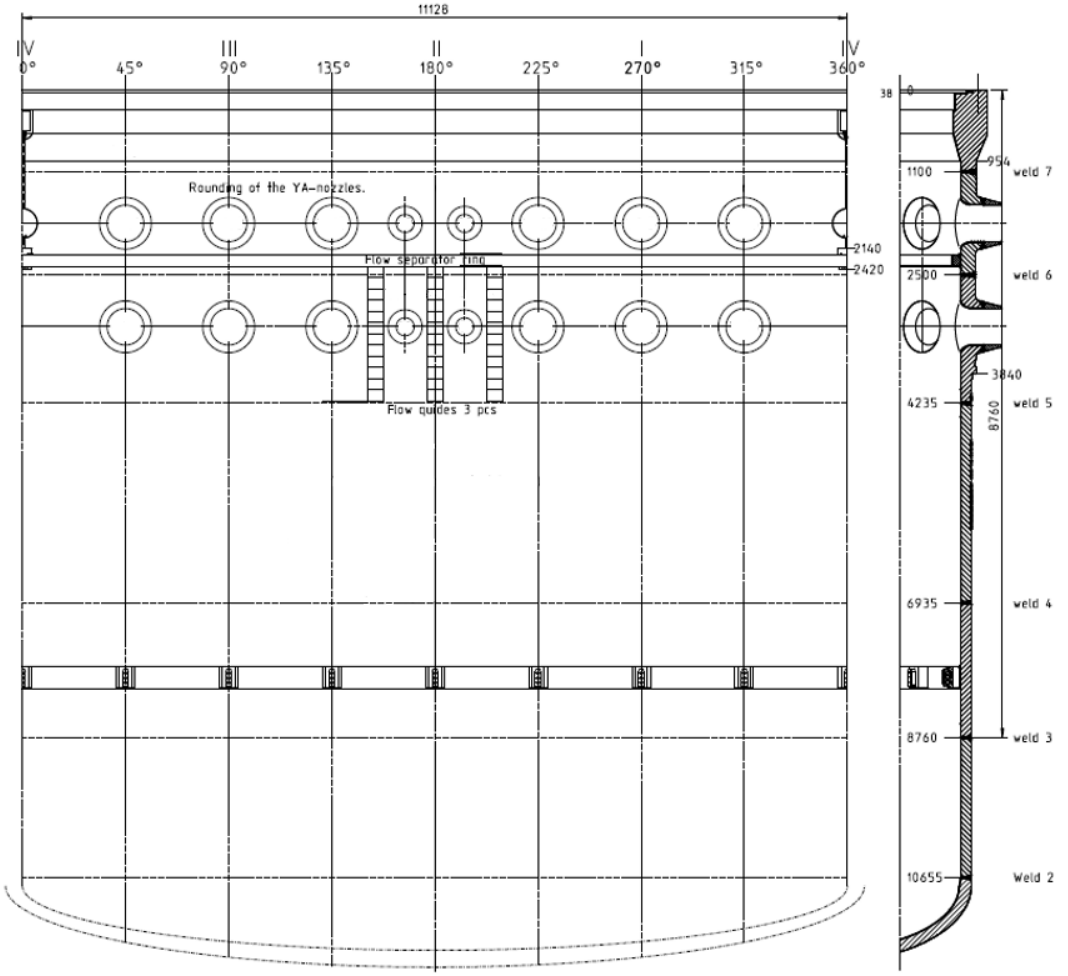

Figure 2. Rolled out overview of LO2 RPV [8]

When the operation of Loviisa NPP was started in 1980's, a surveillance program was commenced for the embrittlement within LO1 RPV. During the surveillance program it was found out that the damage to RPV structure caused by neutrons were higher than expected. This lead to thermal annealing that was performed for LO1 RPV in 1996. In addition to thermal annealing some fuel bundles on the outer rim of reactor core were replaced with dummy elements in order to reduce neutron flux. Remaining fuel bundles were also rearranged for achieving lower leakage for neutron irradiation to the RPV. Same actions with the exception of thermal annealing were taken in LO2 in order to mitigate embrittlement within the RPV. [11]

Due to neutron irradiation the NDT levels in RPV base material and weld material has increased. The NDT values for Loviisa RPV internal and external surfaces have been calculated and taken into account for the PTS studies. [12]

2.3 Postulated rapid cooling of the external side of RPV

One of the overcooling sequences in Loviisa NPP that is studied in Fortum is the rapid cooling on the external side of the RPV by the unexpected start-up of emergency spraying system (TQ-system). It was chosen to be used for thermal insulation studies of this work. The sequence is a result from unexpected start-up of containment emergency spraying system while the NPP is operating at full power. The injected water by the TQ-system accumulates to the lower containment sump. Eventually the water reaches the bottom of reactor cavity through air conditioning channels. Water rises upwards in the 30 cm gap between RPV outer surface and concrete wall while rapidly cooling the side of RPV. The rapid cooling causes thermal shock to the external side of the RPV. If the cooling is strong enough to drop the temperature under NDT levels and there are existing defects within the RPV, the worst case is a fracture occurring through the RPV. [5]

The rising water and the following rapid cooling is causing biggest stress to the weld that is located in the beltline region making it more embrittled location than elsewhere on the external surface of the RPV. In order to increase the effect of thermal shock in the sequence and thus making the study more conservative, the water temperature is assumed to be as low as possible. This is achieved by assuming the accident to happen during winter

with lowest possible sea water temperature and also having pessimistic assumptions for process, e.g. assuming that only one TQ-pump is operating in both redundancies. Before the water by TQ-system is sprayed to the containment it is cooled by intermediate circuit with seawater. Fewer operational TQ-pumps will lead to lower mass flow rate and it will further decrease the temperature of sprayed water. In addition two defects are assumed, where one is located in the internal side beneath the cladding and second one in the external side within the weld. The accident sequence is assumed to last for thirty minutes and then the TQ-system is halted by the operator. [5] The gap between RPV and concrete wall where the water accumulates is illustrated in Figure 3.

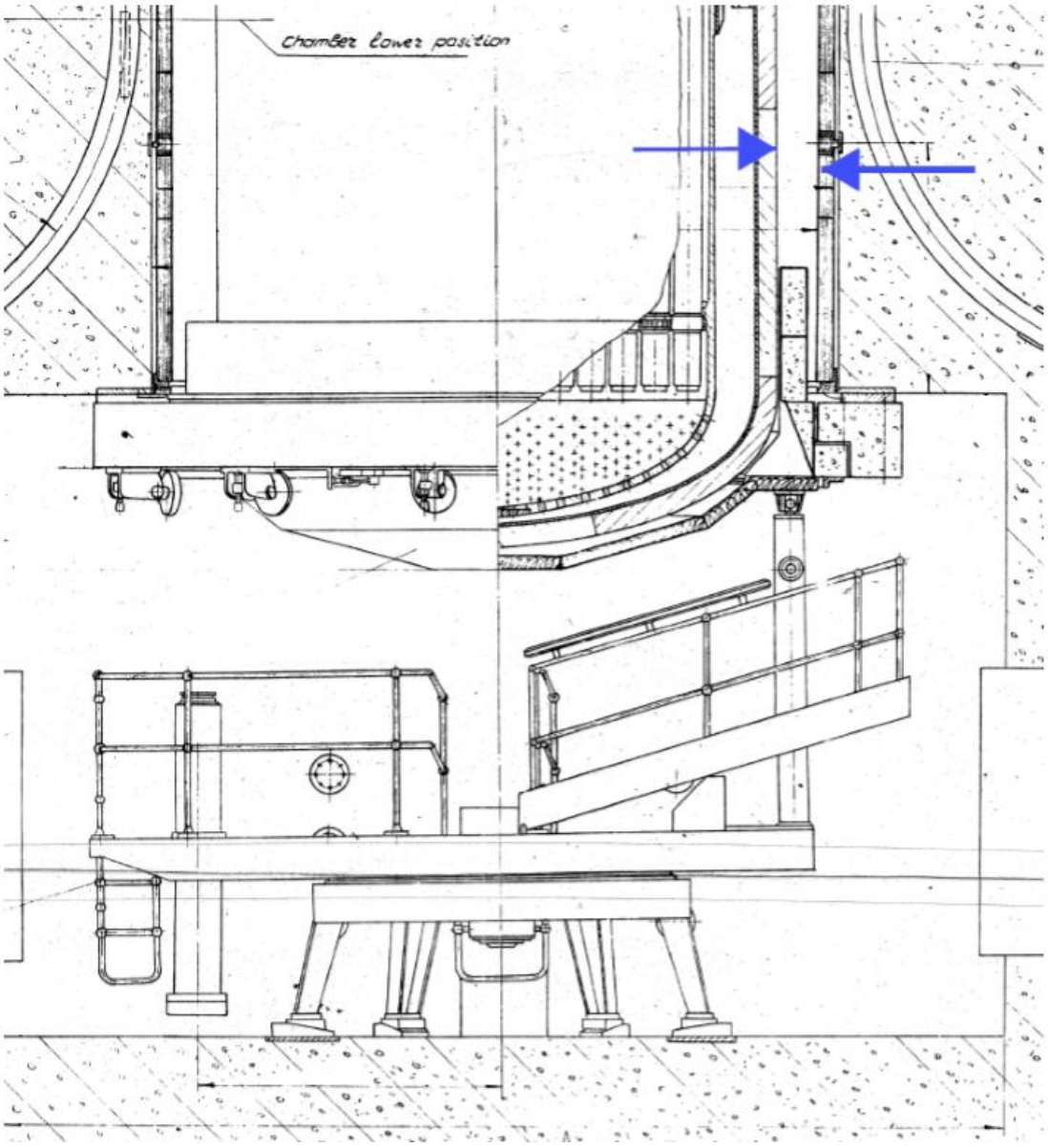

Figure 3. Lower part of the RPV. The gap between RPV outer surface and the concrete wall is shown by blue arrows. [8]

2.3.1 Conditions and transient progression

The TQ-system is assumed to start accidently when the NPP is operating at full power. The sequence lasts for 1800 seconds (30 minutes) and then TQ-system is assumed to be terminated by the operator. The starting conditions that are notable are the following:

- Reactor power 100% (1500 MW)
- Primary circuit pressure in pressurizer about 12.4 MPa
- Water level in pressurizer 4.6 m
- Temperature in hot leg 299.9 °C
- Temperature in cold leg 266.1 °C
- Coolant mass flow in primary circuit about 8500 kg/s
- Temperatures in TQ-lines 16 °C
- Total mass flow in TQ-system 400 kg/s
- Temperature of seawater 0.1°C

Accident sequence has been analyzed by Fortum with APROS process simulation software. [13] Following figures are some of the results from the simulation. The estimation for water elevation in the gap between RPV outer surface and concrete wall is shown in Figure 4.

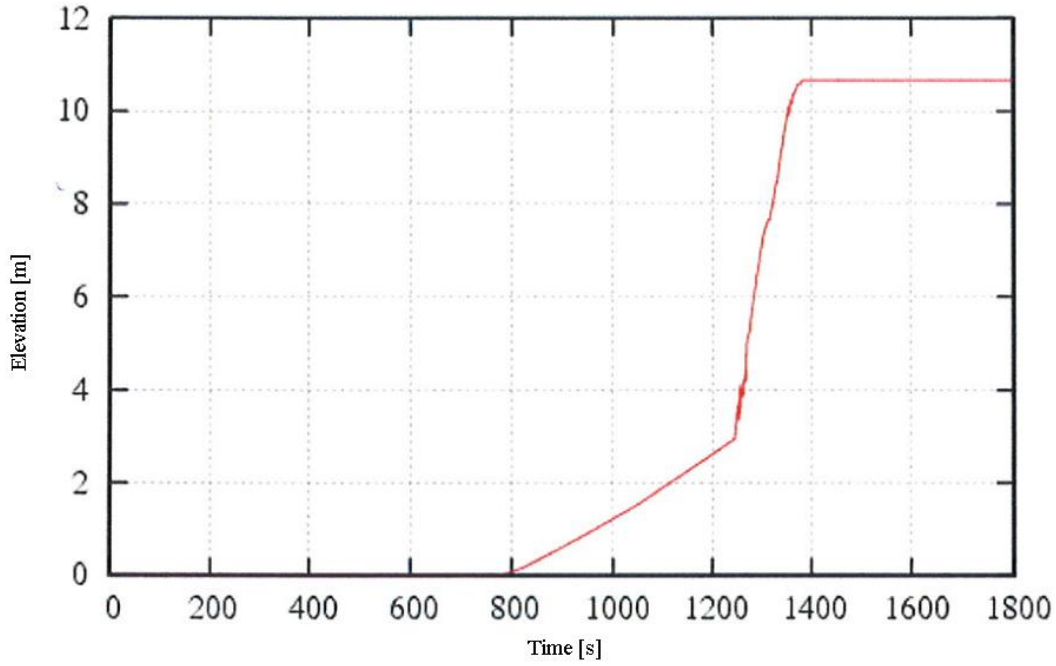

Figure 4. Water level between RPV outer surface and concrete wall in postulated cooling sequence. [13]

The estimation of surface temperature on the weld that is located in the beltline region is shown in Figure 5 and the corresponding heat transfer coefficient from wall to water during the transient is found in Figure 6.

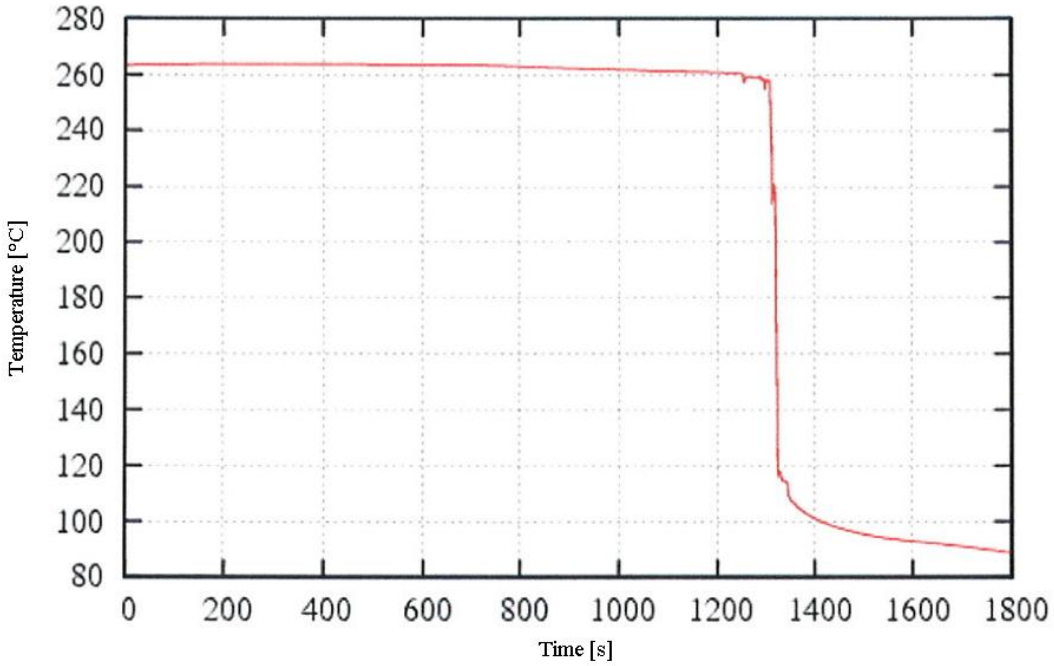

Figure 5. External surface temperature at the weld located in the beltline region. [13]

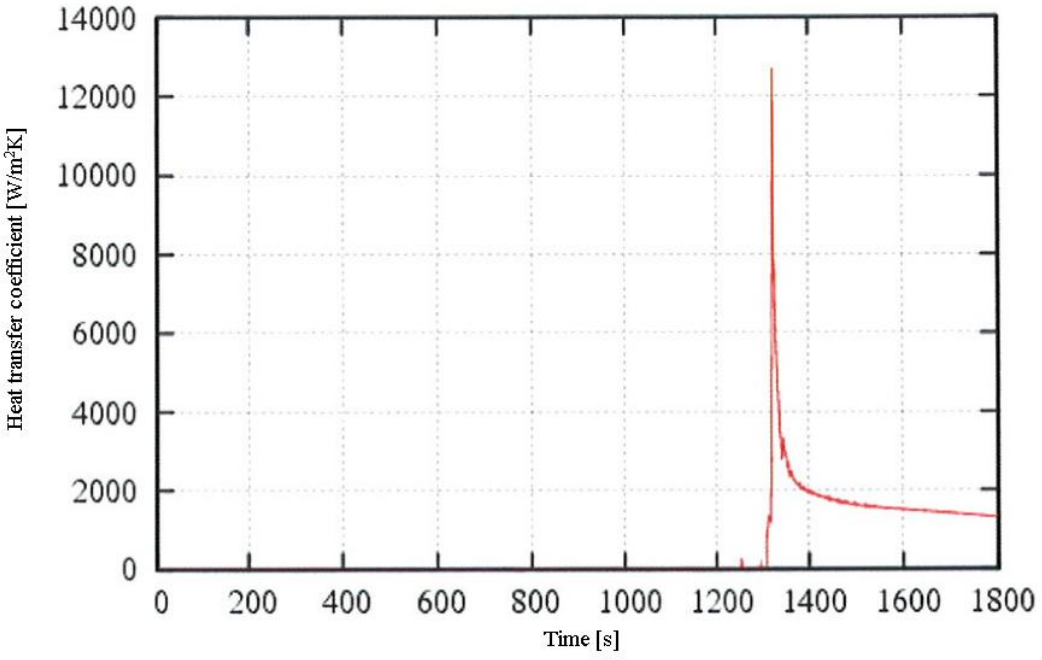

Figure 6. Heat transfer coefficient from RPV surface to water at the weld located in the beltline region. [13]

2.4 Reduction of PTS

Some methods executed in Loviisa NPP in order to reduce PTS were introduced in section 2.2.1. Mitigation of radiation embrittlement leading to slower rising of NDT in the future is an effective preemptive method. The actions taken for the reduction of PTS need to be properly adjusted on specific NPP case by case. This section introduces methods for mitigating PTS.

2.4.1 General methods

General mitigation methods can be roughly divided into two categories. First category includes the methods that are directly or indirectly resulting to better RPV integrity and lower NDT levels. Second category includes methods that are directly reducing or eliminating the risks or probabilities of PTS.

First category that improves the RPV integrity is mostly achieved by reducing the impact of radiation embrittlement. Actions taken in Loviisa that fall in the first category and recommended methods by IAEA include [14, 2]

- Optimizing fuel management by using low leakage core loading pattern in order to reduce neutron flux to the RPV wall.
- Reconfiguration of the core by using partial shielding assemblies or dummy elements such as hafnium or stainless steel to reduce neutron flux at wanted areas of the RPV wall.
- Thermal annealing of the embrittled RPV for the purpose of recovering material integrity.

Overall benefits of neutron flux reduction are depending on time of implementation, original neutron flux levels and chemical composition of RPV material. All mitigation actions should be implemented and researched properly case by case on each considered NPP. [1] Second category includes actions that directly have mitigation impact on PTS:

- Reducing the effect of thermal shock by raising water temperature in ECCS.
- Removing the threat of cold plumes by adjusting the injection of ECCS to primary coolant in a manner that completely mixed flowing conditions are achieved.
- Shut-off head and injection capacity adjustment in high pressure injection pumps.

- Adjustment of steamline isolation procedures.
- Operator training and improvement of the emergency situation instruction manuals regarding PTS risks.

2.4.2 Thermal insulation of sensitive weld

A proposal for more specialized solution for mitigating thermal shock is by thermally insulating most sensitive parts of the RPV. Typically the welds around the beltline region suffer the most from embrittlement. Thermal insulation on internal side of the RPV might be utmost challenging because of more difficult conditions e.g. higher radiation, corrosion, attachment and installation challenges and insulation effect on the existing cladding. However externally the thermal insulation encounters fewer challenges and could therefore be one potential option for reducing the impact of thermal shocks

In the external overcooling cases such as mentioned in section 2.3 the thermal insulation could reduce the thermal shock effectively by mitigating the temperature gradient in the RPV during accident scenarios. Mitigation of temperature gradient in overcooling accident would reduce the stress that existing defects would suffer and it could potentially prevent the possibility of RPV fracture.

Thermally insulating the sensitive weld in the RPV has not been studied before. The further research in this study is focused on the external insulation of the sensitive weld in the RPV. Therefore cases where internal insulation is considered, the results in this study are not completely applicable.

3 THERMAL INSULATION

Heat can be transferred through conduction, convection or radiation. In thermal insulation the goal is to restrict the heat transfer. Thermal insulation can be achieved by different engineered methods and processes or by using suitable materials and different object shapes. [15]

Strong cooling on the outer surface of Loviisa RPV causes high temperature gradient to the surface of RPV wall. In the postulated rapid cooling (see 2.3) the biggest contributors to heat transfer are convection and conduction. Radiation heat transfer also contributes but the impact can be considered minimal (more on the topic in 4.1.2). Studying thermal insulation effect by adding an insulating layer can be studied rather easily by simulations and calculations. Studying other insulation methods that include different object shapes or engineering solutions that restrict the heat transfer will most likely require real experiments.

The thermal insulation by adding an insulating layer will have some requirements due to the challenging conditions outside of the Loviisa RPV. Challenging conditions will set some crucial requirements that need to be taken into consideration. This section focuses on these requirements for materials to achieve acceptable level for being used as thermal insulator.

3.1 Requirements for insulation material

If the thermal insulation is done by adding an insulating layer on the outer surface, a concept of thermal resistance is good indicator. Unit thermal resistance for conduction to x-direction in Cartesian coordinates is defined as

$$R = \frac{\Delta T}{q_x} = \frac{x}{k} \tag{1}$$

where q_x is heat flux, T is temperature and k is thermal conductivity. Unit thermal resistance is approximately valid for round piece of insulation around an RPV because insulation layer is very thin compared to its radius. Different layers of materials can be

summed up in series to create thermal circuits. Convection can also be described as resistance and it can be summed up to the thermal circuit as additional resistance. The summed up thermal circuit provides concept for quantifying the heat transfer. The heat flux is constant throughout the thermal circuit when the observed system is in steady state. Thermal circuit with convection and two layers of different material becomes to

$$q_x = \frac{T_{1,s} - T_{2,s}}{x_1/k_1} = \frac{T_{2,s} - T_{3,s}}{x_2/k_2} = \frac{T_{3,s} - T_\infty}{1/h} \tag{2}$$

where h is heat transfer coefficient for convection and T_∞ is the surrounding fluid temperature.[15, 16]

3.1.1 Thermal conductivity

Thermal conductivity provides indication of the rate at which energy is transferred by diffusion process. Thermal conductivity is strictly a property of material. The effect of thermal conductivity can be understood better mathematically. Using Fourier's law, the thermal conductivity is defined to x-direction as

$$k_x = -\frac{q_x}{(\Delta T/\Delta x)} \tag{3}$$

Foregoing equation states that when prescribed temperature gradient exists, the conduction heat flux increases with increasing thermal conductivity [15].

In a case where thermal conductivity is constant within material and steady state exists, the temperature will change at constant linear rate within the material. Adding different material with different thermal conductivity results the temperature gradients being again linear, but interface temperature between the materials depend on relative values of thermal conductivities and thicknesses [16]. Figure 7 is illustrating interface temperature T_2 between two different materials where the second material is behaving as insulation. The concept of Equation 2 is applicable in the same situation.

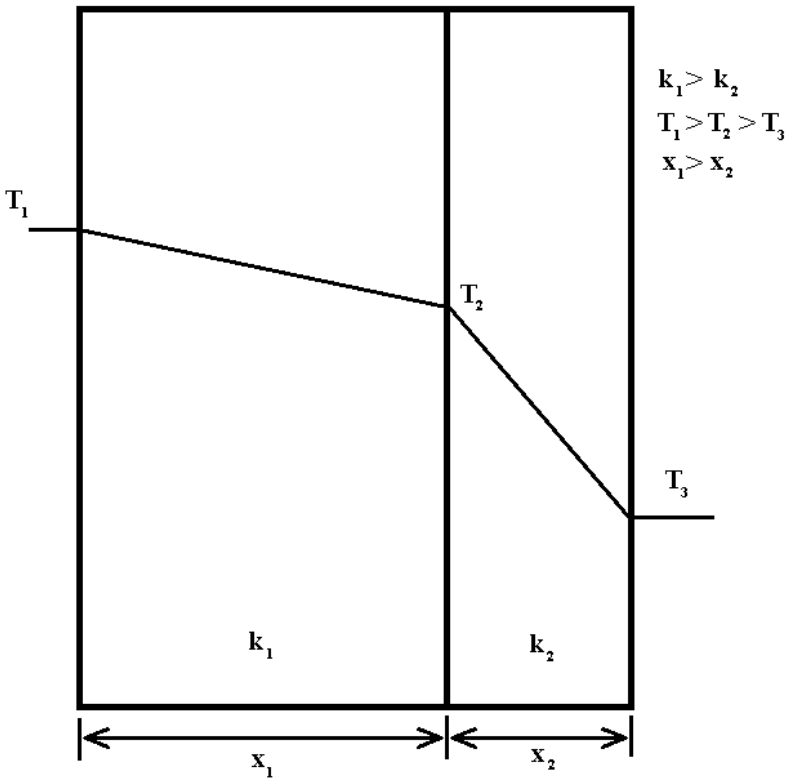

Figure 7. Temperature distribution through a two layer wall in steady state.

Thermal conductivity in Loviisa RPV averages to value of 38 W/m·K under operational temperature. A good thermal insulation has low thermal conductivity or combination of materials with low thermal conductivity. When considering any insulation in Loviisa RPV the recommendable value for thermal conductivity should be less than mentioned value 38 W/m·K, because this will result in higher interface temperature. The materials with higher value for thermal conductivity will drop the interface temperature in longer run, but the aimed mitigation effect during the thermal shock could be achieved if the thermal resistance is high enough with properly adjusted thicknesses.

3.1.2 Thermal diffusivity

Thermal diffusivity is important in transient situations. It describes the ability of material to conduct thermal energy relative to its ability to store thermal energy. Thermal diffusivity is defined as

$$\alpha = \frac{k}{\rho c_p} \tag{4}$$

where ρ is density and c_p is specific heat capacity. Thermal diffusivity has units of m^2/s. Material with low thermal diffusivity responds to changing thermal environment more slowly than material with high thermal diffusivity. [16]

Interpolating the values for operational temperature from Table 1 and placing them in Equation 4 yields

$$\alpha_{\mathrm{rpv}} = \frac{38.2 \frac{\mathrm{W}}{\mathrm{mK}}}{7800 \frac{\mathrm{kg}}{\mathrm{m}^3} \cdot 502 \frac{\mathrm{J}}{\mathrm{kg \cdot K}}}$$

Value for thermal diffusivity of RPV in operational temperature becomes to

$$\alpha_{\mathrm{rpv}} \approx 9.76 \cdot 10^{-6} \frac{m^2}{s}$$

Insulation material with higher density and specific heat capacity along with low thermal conductivity will lead lower value for thermal diffusivity. Material with low thermal diffusivity will take longer time to reach a new equilibrium state. This will be beneficial in the mitigation of PTS.

3.1.3 Temperature resistance

The coolant temperature in the cold leg of Loviisa NPP during full operational power is around 266 °C. In equilibrium state before the transient the fair assumption for uniform temperature within the RPV is the mentioned temperature of coolant. Same assumption can be made for the possible insulation material. Therefore the minimal operational temperature requirement for any insulation material should be higher than the uniform temperature. Any phase transition is not allowed for the insulation material.

3.1.4 Radiation resistance

Fortum has researched and simulated the exposure of high energy neutrons within the RPV. Simulation program PREVIEW synthesizes neutron flux in pre selected locations within the RPV. With PREVIEW it is possible to take into account already occurred and the anticipated history of reactor power, power distribution and burnup rate in each cycle. PREVIEW has been used as a tool to monitor the accumulation of neutron doses until the year 2010 by using real operational data. After 2010 the PREVIEW simulations have continued to simulate accumulation of neutron doses up until 2027. [17]

The following has been taken into consideration in dose calculations: the dampening of dose from internal side to external side, 15mm deep postulated defect's influence on maximum dose and the possible correction for dose based on conducted measurements. The expected maximum neutron dose for the external and internal defects in the beltline region between the years 2017-2027 are found in Table 2. The threshold energy in the RPV for neutron dose is 1 MeV. [14]

Table 2. Expected neutron dose at the beltline region between years 2017-2027 (E>1.0MeV).

Location	**n/cm^2**
Internal defect	$8.6 \cdot 10^{18}$
External defect	$2.3 \cdot 10^{18}$

The thermal insulation should withstand the doses portrayed in previous table. More precisely the thermal insulation will be installed on the external side of the RPV so the minimum threshold should be higher than the dose on the external defect. Neutron dose will in reality be further dampened to the external surface but conservatively the value found in Table 2 can be set to be the limit. It is important for insulation material to be able to withstand the neutron influence since the thermal insulation will almost immediately start to suffer from embrittlement once installed.

3.1.5 Versatility and durability

The thermal insulation material should have good versatility and it should be able to withstand stresses. Due to challenges in installing the thermal insulation a machinable material is recommendable. The durability is required for the thermal insulation since it should be able to withstand harsh environment until the end of the NPP's lifetime. The installed thermal insulation should stay intact and withstand accident scenarios without falling off.

Resistance to water is needed. It is unacceptable for the material to start deforming or dissolving after having a contact with water. Loose and detached parts due to wetting may cause unacceptable clogging to occur.

3.1.6 Corrosion effect

Galvanic corrosion occurs when a metallic contact is made between less noble metal and more noble metal. Galvanic corrosion rate increases in more moisture atmosphere. However the corrosion effect is nonexistent in warm and dry environments. [18] The atmosphere surrounding the external side of the RPV is in high temperature and low humidity. The corrosion effect between RPV and possible insulation can therefore be assumed to be minimal.

3.1.7 Optimization of thermal insulation thickness

Thermal insulation thickness should be optimized. Thinner thermal insulation leads to weaker integrity, durability and in addition the desired result in thermal shock mitigation may not be achieved. Too thick thermal insulation may lead for the strong heat transfer taking place in the edging of the thermal insulation, leading to undesirable heat transients. Too thick thermal insulation also influences on the machinability and versatility of the material. The maximum thickness is restricted by the gap between the RPV outer surface and concrete wall which is 30cm.

Optimization of thermal insulation thickness greatly depends on the material properties and

each material thickness optimization should be taken into consideration individually.

3.2 Thermal insulation methods

The thermal insulation should cover the whole outer surface of the sensitive weld. This will make the thermal insulation to be circular following along the welded seam. Therefore the thermal insulation is likely to be ring shaped in order to cover the whole area of the welded seam.

Other proposed methods are using different object shapes in a purpose of preventing or disrupting the contact between water and sensitive weld. This would require maze-like-structures or metallic-wools.

3.3 Attachment

The access to outer surface of the RPV is very limited. There are two small opening hatches below the RPV for inspection purposes. The total length of the opening hatches is 700mm and the width is approximately 300mm. A manipulator system is used for inspection. The system includes arc guidance, probe holder, mast for lifting the probes and rotating table. [8] This manipulator system can potentially be used when installing the thermal insulation.

3.4 Rejected insulation materials

Main cause for rejection has been the material's poor radiation resistance or incompatible operational temperature. Following materials do not pass the criteria:

- Polytetrafluoroethylene (PTFE) also known as Teflon. PTFE has very ideal material properties but it suffers severe damage after relatively small amount of radiation. [19]
- Polyurethane is hydrocarbon thermoplastic with excellent insulator properties and acceptable radiation resistance. Polyurethane's is rejected due to its lack with maximum operational temperature which is around 120 °C.
- Both epoxy and phenolic withstand radiation well but lack in the

operational temperature.

- Materials with higher concentration of manganese, phosphorous, nickel, vanadium or copper due to increased damage of irradiation. [2]
- Paints and adhesives are rejected due to weak resistance to radiation damage or temperature. [19]
- Rubbers are rejected due to lack with operational temperature and radiation resistance. [19]
- Materials that deform or become degradable when contact with water is established (e.g. wool).

3.5 Potential insulation materials

3.5.1 MACOR™

Macor™ is glass ceramic for industrial applications that is extremely machinable, withstands high temperatures by remaining continuously stable at 800 °C. It also has low thermal conductivity and diffusivity and it is radiation resistant. Thermal properties of Macor™ are listed in Table 3. The typical applications include aerospace and nuclear installations. [20]

Table 3. Thermal properties of Macor™ [20]

Parameter		Unit	Value
Specific heat, 25 °C	c_p	J/kgK	790
Thermal conductivity, 25 °C	k	W/mK	1.46
Thermal diffusivity, 25 °C	α	m^2/s	$7.3 \cdot 10^{-7}$
Maximum no load temperature		°C	1000

3.5.2 Calcium silicate

Calcium silicates withstand high temperatures and they generally have low and stable thermal conductivity values. Calcium silicates provide excellent structural integrity and it enables good machinability characteristics for complex structures. Calcium silicates have excellent resistance and stability for thermal shocks. Figure 8 is a 3D graph comparing density, bending strength and thermal conductivity between structural calcium silicates.

The structural calcium silicates are available in large sizes and they can be machined for customer's specification. [21]

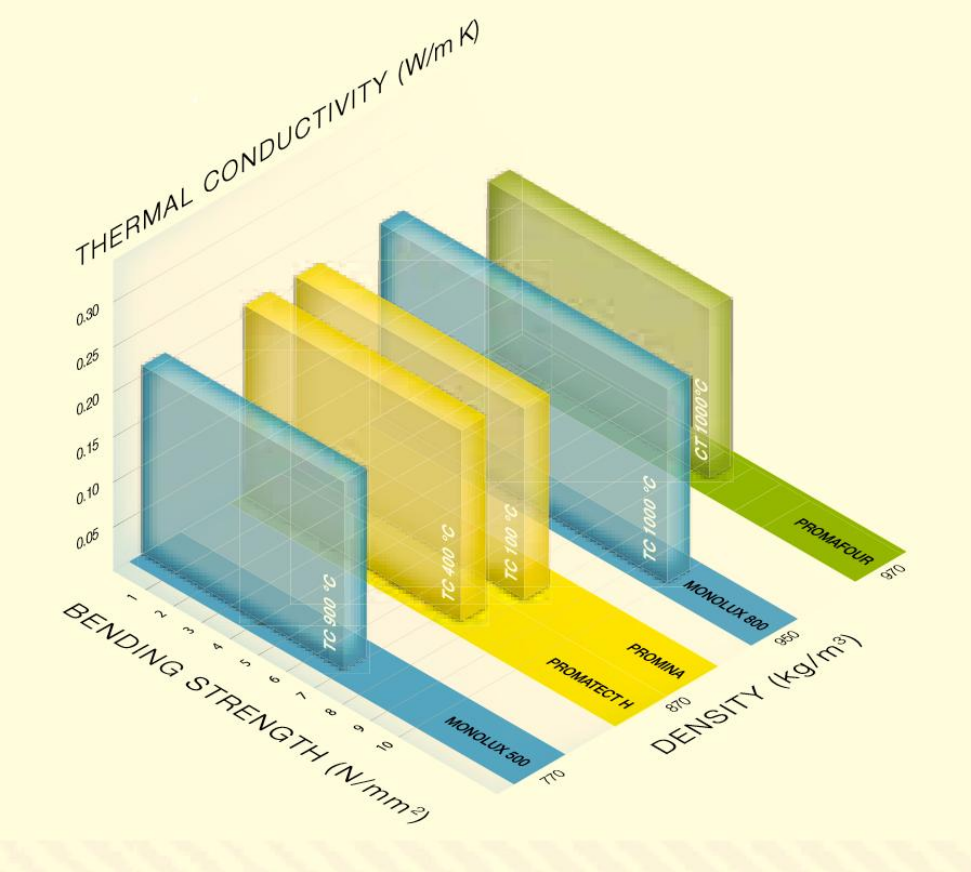

Figure 8. Thermal conductivity, density and bending strength comparison for structural calcium silicates. [21]

There are varieties of calcium silicates with different properties. Table 4 contains the averaged properties to a certain extent which have been used in calculations for giving averaged perspective. Silicate which is anionic silicon compound influences on irradiation sensitivity. [2] Calcium silicate can withstand the accumulated neutron dose on the external side of the Loviisa RPV for 10 years before suffering mild to moderate damage. For longer period the Calcium silicate is not a solution.

Table 4. Thermal properties of typical calcium silicate.

Parameter		**Unit**	**Value**
Specific heat, 0-100°C	c_p	J/kgK	1030
Thermal conductivity, 265°C	k	W/mK	0.32
Thermal diffusivity, 265°C	α	m^2/s	$4.01 \cdot 10^{-7}$

Melting range	°C	1000

3.5.3 Stainless steel AISI316

Stainless steels have good radiation resistance. Stainless steels overall possess very similar thermal properties as the RPV material with an exception of lower thermal conductivity. All the requirements are passed but the thermal insulation effect might not be enough with small thicknesses. Table 5 contains thermal properties of stainless steel AISI316. [22]

Table 5. Thermal properties of AISI 316. [22]

Parameter		**Unit**	**Value**
Specific heat, 0-100 °C	c_p	J/kgK	500
Thermal conductivity, 265 °C	k	W/mK	18.345
Thermal diffusivity, 265 °C	α	m^2/s	$4.592 \cdot 10^{-6}$
Melting range		°C	1371-1399

3.5.4 Titanium Ti-6Al-4V

Ti-6Al-4V has low thermal conductivity when compared to other metals. Ti-6Al-4V has high melting point and good radiation resistance even though it has small concentration of vanadium. It is also machinable making it generally pass all the requirements. Table 6 contains the thermal properties of Ti-6Al-4V [23]

Table 6. Thermal properties of Titanium Ti-6Al-4V. [23]

Parameter		**Unit**	**Value**
Specific heat, 0-100 °C	c_p	J/kgK	565
Thermal conductivity, 265 °C	k	W/mK	6.6
Thermal diffusivity, 265 °C	α	m^2/s	$2.637 \cdot 10^{-6}$
Melting range		°C	1650

3.5.5 Zirconium

Zirconium has widely been used as structural materials in reactors. Zirconium has good radiation resistance and it has low thermal conductivity for a metal. There is variety of zirconium alloys, but pure zirconium was chosen to be used in the calculations. [24] Table 7 contains the thermal properties of zirconium.

Table 7. Thermal properties of Zirconium [15]

Parameter		**Unit**	**Value**
Specific heat, 27 °C	c_p	J/kgK	278
Thermal conductivity, 27°C	k	W/mK	22.7
Thermal diffusivity, 27°C	α	m^2/s	$1.24 \cdot 10^{-5}$
Melting range		°C	2125

4 TEMPERATURE DISTRIBUTION ANALYSIS

Temperature distribution analysis for different depths at different time steps during each transient is required for understanding RPV integrity during PTS transients. In general the boundary conditions are nonlinear, for example heat transfer coefficient can be a function of surface temperature thus making the heat transfer analysis nonlinear as well. Boundary conditions, material properties, thermal conductivity, specific heat and density of materials must be defined for transient PTS problems. In uncoupled heat transfer analysis the deformations of RPV structure are not taken into consideration, making thermal expansion coefficients unnecessary. [4]

Temperature distribution analysis can efficiently determine insulation's effect on the external side of RPV during PTS transient. Reduced temperature distributions are used to estimate the mitigation of stress distributions and their impact on the integrity of RPV. For solving the temperature distributions, appropriate conservation equation has to be determined for each nodal points of unknown temperature. Heat conduction equation can be used for a system with no internal generation and with a uniform thermal conductivity. Finite-difference equations can be derived from heat equation in the case where system is characterized in terms of a nodal network. [15]

Matlab script was developed for solving the temperature distributions within the RPV during external transient cooling. Following section explains assumptions made, correlations used, nodalization and validation of the Matlab script.

4.1 Assumptions

Many factors influence on the uncertainty in calculations. Especially estimating accurate heat transfer coefficient on the outer surface of RPV during intense external cooling is challenging without any experimental data for comparison. Fortunately heat transfer experiments on external cooling were performed at LUT in 2008. [25] Assumptions are needed for simplifying some aspects in the calculations. Results and observations from these heat transfer experiments had influence on the assumptions and simplifications for the Matlab script. They were also partly used as validation for the developed script.

4.1.1 Vertical plate

For performing the heat transfer experiments in LUT, a test facility with vertical plate was constructed. Simplifying the case from cylindrical RPV to vertical plate makes the observation of the case much simpler. This simplification is possible and very acceptable since the RPV is axially symmetric at the core level and the curvature of the RPV can be ignored due to the huge ratio between vessel radius and wall thickness. The observation of heat transfer due to this simplification is focused on a small sector of the RPV but the experimental results can be applied to all sectors as a whole. [25]

The Matlab script has same assumption as a basis. The observed part of the RPV is assumed to be vertical plate in rectangular sector. Moreover the calculations for the temperature distribution within the RPV wall are done one-dimensionally. The thickness for the plate will be the same as the RPV thickness including the cladding. Even though the inner cladding has different material properties than the RPV base material, overall the inner cladding has insignificant effect on cooling of the outer surface. The material in the calculations for whole thickness is set to be base material of the RPV. The characteristic length in the calculations was set to be constant 10cm so it would cover the weld completely.

4.1.2 Transient progression in calculations

During the heat transfer experiments, the boiling transient was observed to be very intense and only lasting for a few seconds. [25] Determining the boiling regime accurately is challenging due to very fast intense boiling. The typical boiling curve for water can be seen in Figure 9.

Boiling regime is determined by the difference between surface temperature and the saturation temperature. In a very intense and only a moment lasting boiling, the regime can be assumed to settle around critical heat flux (CHF) with a combination of nucleate boiling and transition boiling. Post-CHF heat transfer is encountered when temperature on the surface is too high to maintain a continuous liquid contact. In transition boiling the surface becomes covered by occasional vapour blanket and heat transfer becomes less efficient until to the point of minimum heat flux is reached (point D in Figure 9). After the minimum heat flux the vapour blanket becomes more continuous as the film boiling

regime settles in. In film boiling the radiation heat transfer becomes more significant part of the heat transfer as the temperature of the wall increases. During the intense transient the heat transfer modes can succeed each other in the same locations during same time. [26]

The conclusion in the external cooling experiments was that some film boiling could also be present at the beginning of the transition but it will not last for long since the surface temperature will not able to maintain it due to strong quenching. [25] Film boiling contribution can therefore be assumed to be minimal.

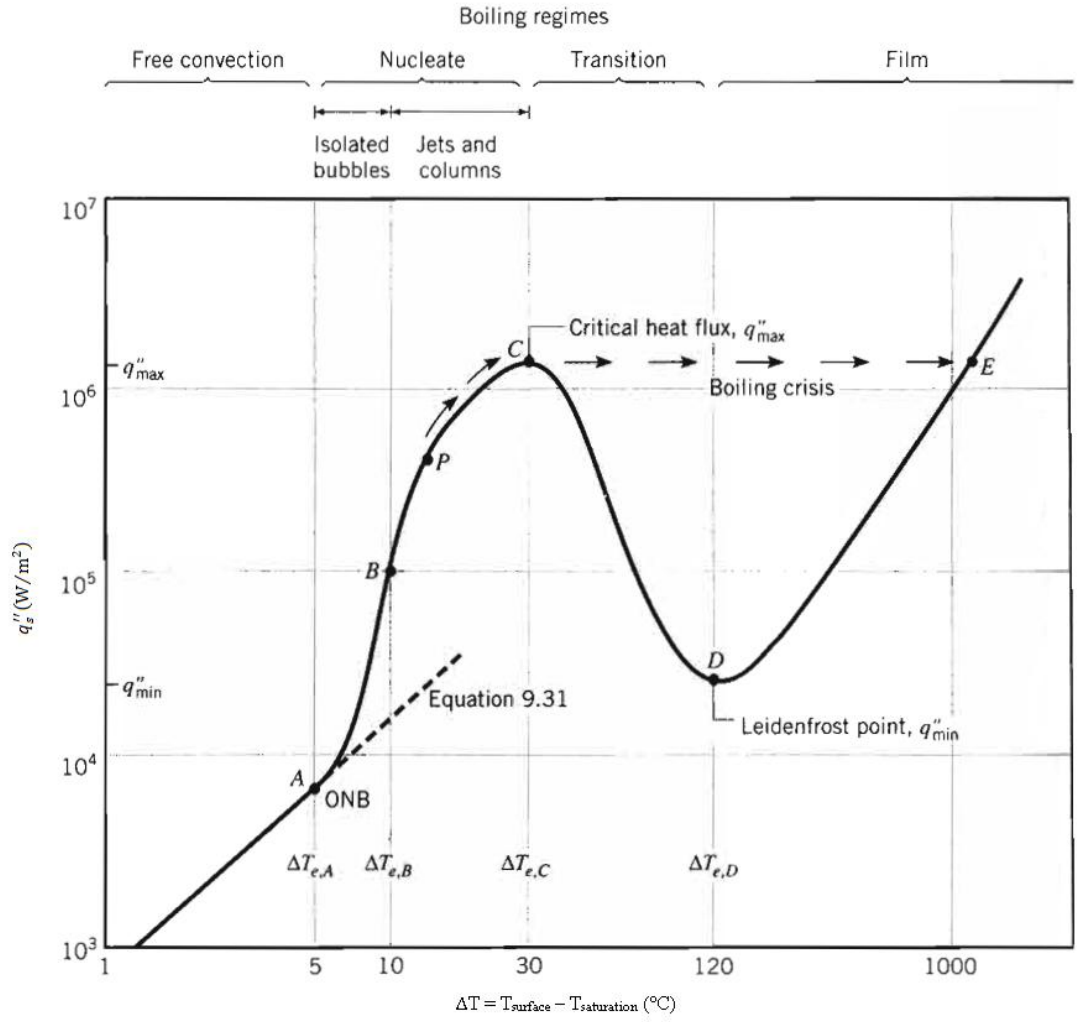

Figure 9. Typical boiling curve for water at atmospheric pressure. The surface heat flux being a function of excess temperature. [15]

A single correlation for the heat transfer coefficient cannot handle the whole boiling process by itself. Correlation used to describe the intense transient boiling will be combination of correlations. The strongest gradients for temperature difference will

emerge if CHF is used during the intense cooling. Conservatively this could be used when surface temperatures exceed the point for CHF. This would also simplify the calculations by eliminating correlations for post-CHF boiling regimes.

4.1.3 Contact resistance

In combined systems, the contact resistance causes temperature drop between combined materials. Contact resistance is principally caused by surface roughness effects between the surfaces. Rougher surface means more gaps that contribute more to the contact resistance. When contact resistance is assumed to be insignificant, the assumption makes the surfaces of both combined material completely smooth. Heat is transferred through contact spots that govern all the contact area. [15, 16]

The contact resistances between multiple materials are hard to define accurately in advance, especially when the contact resistance is not significant. In calculations the contact resistance is assumed to be negligible between the thermal insulation layer and RPV surface in order to simplify the calculations.

4.2 Correlations

Heat transfer coefficient on the outer surface is difficult to define precisely as mentioned in section 4.1.2. Generally the heat transfer coefficient from wall surface to coolant can be expressed by Newton's law of cooling [15]

$$h = \frac{q_x}{(T_w - T_\infty)} \tag{5}$$

where T_w is wall temperature. In the course of developing the Matlab script, multiple correlations were considered. Chen correlation for boiling in an upward vertical tube gave the most promising results when calculations were compared to experimental results. Therefore it ended being used as one of the boiling correlation. Chen correlation is divided into two parts that combine nucleate boiling and convective contribution. The basic form of Chen correlation is defined as [27]

$$h_{tp} = h_{fz}S + h_{db}F \tag{6}$$

where h_{fz} is Foster-Zuber correlation for nucleate pool boiling, S is nucleate boiling suppression factor, h_{db} is Dittus-Boelter correlation for convective heat transfer and F is convective boiling factor. The Foster-Zuber correlation for nucleate pool boiling coefficient is defined as [28]

$$h_{fz} = 0{,}00122\left[\frac{k_L^{0,79}c_{pL}^{0,45}\rho_L^{0,49}}{\sigma^{0,5}\mu_L^{0,29}h_{LV}^{0,24}\rho_V^{0,24}}\right][T_w - T_{sat}(p_L)]^{0,24}[p_{sat}(T_w) - p_L]^{0,75} \tag{7}$$

where σ is surface tension, μ_L is liquid viscosity, h_{LV} is heat of vaporization, T_{sat} is saturation temperature and p is pressure. The Dittus-Boelter single-phase heat transfer coefficient for liquid is defined as

$$h_{db} = 0{,}023Re_L^{0,8}Pr_L^{0,4}\left(\frac{k_L}{D_H}\right) \tag{8}$$

Where the Re_L is liquid Reynolds number, Pr_L is liquid Prandtl number and D_H is hydraulic diameter. The liquid Reynolds number is expressed as

$$Re_L = \frac{\dot{m}(1-X)D_H}{\mu_L} \tag{9}$$

where $\dot{m}$ is total mass flow and X is the local vapor quality. The liquid Prandtl number is defined as

$$Pr_L = \frac{c_{pL}\mu_L}{k_L} \tag{10}$$

The convective boiling factor is obtained by [27]

$$F = \begin{cases} 1, & X_{tt}^{-1} \le 0{,}1 \\ 2{,}35\left(\frac{1}{X_{tt}} + 0{,}213\right)^{0,736}, & X_{tt}^{-1} > 0{,}1 \end{cases} \tag{11}$$

where Xtt is Lockhart-Martinelli parameter and it is expressed as

$$X_{tt} = \left(\frac{1-X}{X}\right)^{0,9} \left(\frac{\rho_V}{\rho_L}\right)^{0,5} \left(\frac{\mu_L}{\mu_V}\right)^{0,1} \tag{12}$$

The remaining nucleate boiling suppression factor S is expressed as

$$S = \frac{1}{1 + 2{,}53 \cdot 10^{-6} Re_{tp}^{1,17}} \tag{13}$$

where Re_{tp} is local two-phase Reynolds number and it is defined as

$$Re_{tp} = Re_L F^{1,25} \tag{14}$$

Chen correlation is not suitable when the surface temperature drops below saturation temperature or surface temperature exceeds the temperature point for CHF. Fortum developed heat transfer coefficient correlation for post boiling based on one of the heat transfer experiments carried out at LUT. The correlation is effective when the surface temperature is below saturation temperature. The developed heat transfer coefficient is defined as [28]

$$h = \begin{cases} h_1, & h_1 = h_{cc} + b \quad when \quad T_w < T_{sat} \quad and \quad h_1 \geq h_2 \\ h_2, & h_2 = a \cdot h_1 \quad when \quad T_w < T_{sat} \quad and \quad h_2 > h_1 \end{cases} \tag{15}$$

where h_{cc} is Churchill-Chu heat transfer correlation for external flow on vertical plane, b and a are constants. The Churchill-Chu correlation is defined as

$$h_{cc} = \frac{k}{L}\left(0{,}825 + \frac{0{,}387 Ra_L^{1/6}}{\left(1 + \left(\frac{0{,}492}{Pr}\right)^{9/16}\right)^{8/27}}\right)^2 \tag{16}$$

where Ra_L is Rayleigh number and L is characteristic length. The Rayleigh number is defines as

$$Ra_L = \frac{g\beta(T_w - T_\infty)L^3}{\nu\alpha} \tag{17}$$

where g is acceleration due to gravity, β is thermal expansion coefficient and ν is kinematic viscosity. The constants in the developed heat transfer coefficient correlation are expressed

as

$$\begin{cases} a = 9{,}15295 \cdot 10^{-4}(T_w - T_{sat})^2 + 0{,}06415(T_w - T_{sat}) + 2 \\ b = 215 \end{cases} \quad (18)$$

Originally the heat transfer coefficient by Fortum (Equation 15) was developed for surface temperatures below the saturation temperature. Combining the correlation with Chen correlation gave good agreement with experimental results when the applied temperature range in the Fortum correlation for post boiling was increased by five degrees above the saturation temperature.

4.3 Matlab script

Matlab script started from the use of heat conduction equation. When the thermal conductivity is constant, the heat conduction equation is defined as [15]

$$\frac{\partial^2 T}{\partial x^2} + \frac{\partial^2 T}{\partial y^2} + \frac{\partial^2 T}{\partial z^2} + \frac{\dot{q}}{k} = \frac{1}{\alpha}\frac{\partial T}{\partial t} \quad (19)$$

Heat equation is often simplified, depending on the case at hand. In the developed Matlab script the case is built to be one-dimensional and the heat is transferred solely on *x* direction. In one-dimensional case under transient conditions with properties being constant and without internal generation, the form of Equation 19 becomes to

$$\frac{1}{\alpha}\frac{\partial T}{\partial t} = \frac{\partial^2 T}{\partial x^2} \quad (20)$$

Central-difference approximation is used on Equation 20 to obtain finite-difference form for spatial derivative. Subscript *n* is used to nominate the location *x* of the discrete nodal points. The spatial derivative approximation in equation 20 is described as

$$\left.\frac{\partial^2 T}{\partial x^2}\right|_n \approx \frac{T_{n+1} + T_{n-1} - 2T_n}{(\Delta x)^2} \quad (21)$$

Superscript p is used in discretized form of time. It denotes the time dependence for temperature. It is defined as

$$t = p\Delta t \tag{22}$$

where Δt is timestep. Finite-difference approximation to the time derivative in Equation 20 is expressed as

$$\left.\frac{\partial T}{\partial t}\right|_n \approx \frac{T_n^{p+1} - T_n^p}{\Delta t} \tag{23}$$

Finite-difference approximations are applied with implicit finite-difference scheme. When comparing the implicit method with explicit method, the implicit method has the advantage of being unconditionally stable. In the implicit method temperatures are evaluated at the new time step (p+1), instead of the previous time (p). Temperature of the node depends on the new temperatures of adjoining nodes, which in general are unknown. The corresponding temperatures for adjoining nodes at new time step must be solved simultaneously. To solve these equations one can use for example, Gauss-Jordan method, Gauss-Seidel iteration method, Gauss elimination method, over relaxation method or matrix inversion method. [30]

For example, the implicit form for finite-difference equation for the interior node after combining finite-difference approximations, Equations 23 and 21 in Equation 20 becomes to

$$\frac{1}{\alpha}\frac{T_n^{p+1} - T_n^p}{\Delta t} = \frac{T_{n+1}^{p+1} + T_{n-1}^{p+1} - 2T_n^{p+1}}{(\Delta x)^2} \tag{24}$$

In one-dimensional equation the system to be solved is tri-diagonal. Discrete nodal points are divided for first node, last node and interior nodes. For obtaining the best result it is recommendable to carry out the calculations with small values of Δx and Δt. In the built matlab script, the number of nodes and simultaneously the values of Δx were determined

by the thickness of simulated insulation. Typically number of nodes (N) varied between 500-1500. Rearranging Equation 24 and adding first and last nodal points, the implicit form of the finite-difference equation for the nodes are

$$\begin{cases} k\dfrac{\left(T_{bc}^{p+1}-T_{n}^{p+1}\right)}{2\Delta x}-k\dfrac{\left(T_{n}^{p+1}-T_{n+1}^{p+1}\right)}{\Delta x}=\rho c_p\dfrac{\Delta x}{2}\dfrac{\left(T_{n}^{p+1}-T_{n}^{p}\right)}{\Delta t}, & n=1 \\ k\dfrac{\left(T_{n-1}^{p+1}-T_{n}^{p+1}\right)}{\Delta x}-k\dfrac{\left(T_{n}^{p+1}-T_{n+1}^{p+1}\right)}{\Delta x}=\rho c_p\Delta x\dfrac{\left(T_{n}^{p+1}-T_{n}^{p}\right)}{\Delta t}, & 2\le n\le N-1 \\ k\dfrac{\left(T_{n-1}^{p+1}-T_{n}^{p+1}\right)}{\Delta x}-h\left(T_{\infty}^{p+1}-T_{n}^{p+1}\right)=\rho c_p\dfrac{\Delta x}{2}\dfrac{\left(T_{n}^{p+1}-T_{n}^{p}\right)}{\Delta t}, & n=N \end{cases} \quad (25)$$

where T_{bc} is boundary condition for temperature in the first node. Biot number is dimensionless parameter and it is essential to transient conduction problems that have surface convection. Biot number relates the temperature drop in the solid to temperature difference between solid surface and the surrounding fluid. [15] Biot number is defined as

$$B_i=\frac{h\Delta x}{k} \quad (26)$$

Fourier number is a dimensionless time that is used along with Biot number in transient conduction problems. [15] Fourier number is defined as

$$F_o=\frac{\alpha\Delta t}{\Delta x^2} \quad (27)$$

When applying Fourier and Biot numbers on Equation 25 and rearranging it, the corresponding implicit form of the finite-difference equation for the nodes in one-dimensional system has the form

$$\begin{cases} -F_oT_{bc}^{p+1}+(1+3F_o)T_{n}^{p+1}-2F_oT_{n+1}^{p+1}=T_{n}^{p}, & n=1 \\ -F_oT_{n-1}^{p+1}+(1+2F_o)T_{n}^{p+1}-F_oT_{n+1}^{p+1}=T_{n}^{p}, & 2\le n\le N-1 \\ -2F_oT_{n-1}^{p+1}+(1+2B_iF_o+2F_o)T_{n}^{p+1}-2B_iF_oT_{\infty}^{p+1}=T_{n}^{p}, & n=N \end{cases} \quad (28)$$

This can be used for the RPV without thermal insulation. When adding the thermal insulation layer in the model, it requires some adjustment in the interface node. The temperature in the interface is assumed to be infinitely close on both sides. With assumption that the heat flux across this interface is equal, simple averaging of adjacent node properties is used. The interface node has the form

$$-\bar{F}_{o,n-1}T_{n-1}^{p+1} + \left(1 + \bar{F}_{o,n-1} + \bar{F}_{o,n+1}\right)T_n^{p+1} - \bar{F}_{o,n+1}T_{n+1}^{p+1} = T_n^p \tag{29}$$

where $\bar{F}_o$ is the effective Fourier number gained by averaging heat capacity and density of the interface materials. The adjacent node thermal conductivities are used separately.

Matrix inversion method is used to solve the temperature distributions. System has as many equations as the number of nodes. Matrix inversion method defines these equations as

$$\begin{matrix} a_{11}T_1 + a_{12}T_2 + \cdots + a_{1N}T_N = C_1 \\ \vdots \quad \vdots \quad \vdots \quad \vdots \vdots \vdots \quad \vdots \quad \vdots \vdots \\ a_{N1}T_1 + a_{N2}T_2 + \cdots + a_{NN}T_N = C_N \end{matrix} \tag{30}$$

Where the quantities *a* and *C* are known coefficients consisting of border conditions, Biot number and Fourier number. With matrix notation previous Equation 26 is defined as

$$[A][T] = [C] \tag{31}$$

where

$$A = \begin{bmatrix} a_{11} & \cdots & a_{1N} \\ \vdots & \ddots & \vdots \\ a_{N1} & \cdots & a_{NN} \end{bmatrix} \qquad T = \begin{bmatrix} T_1 \\ \vdots \\ T_N \end{bmatrix} \qquad C = \begin{bmatrix} C_1 \\ \vdots \\ C_N \end{bmatrix}$$

The elements in matrix [A] are a square of the total amount of nodes (N^2). Matrices [T] and [C] are column vectors. The temperature column vector in Equation 31 is solvable by inverting the coefficient matrix [A].[15, 30] Temperature vector is expressed as

$$[T] = [A]^{-1}[C] \quad (32)$$

The developed Matlab script solves temperature distributions by using the mentioned matrix inversion method. Even though the implicit method is stable, it was observed that bigger values for time step caused some oscillation at the interface temperature where correlations were changed. Smaller values for time step eliminated the oscillation completely. The default time step in the simulations was set to be 0.01 seconds.

4.4 Matlab script validation

In order to make sure that the developed Matlab script performs well, it has to be validated. The validation can be expressed as how accurate the script's predictive capabilities for specific output quantities are when compared to theoretical formulas or measured experiments. Validation is typically done by comparing calculated results with real experimental data or by building similar model using reliable simulation programs and then comparing the gained results. [1]

The developed Matlab script was validated by real experimental data [25] and by simulating specified case with FLUENT CFD-simulation program.

4.4.1 Validation by FLUENT simulation

The FLUENT simulation was carried out by Fortum. The objective was to calculate temperature distributions in preselected locations within RPV wall. In both simulations the starting uniform temperature for the wall was selected to be 255 °C. Other boundary conditions and values for material properties were set to be the same. Temperatures in both simulations were calculated in the following points: surface, 5, 10, 20 and 30mm from surface. Heat transfer coefficient from surface to water was set to be dropping stepwise with the following time:

- 0-1s, h=8000 W/(m^2·K)
- 1-2s, h=7000 W/(m^2·K)
- 2-3s, h=6000 W/(m^2·K)

- 3-4s, h=5000 W/(m^2·K)
- 4-5s, h=4000 W/(m^2·K)
- 5-6s, h=3000 W/(m^2·K)
- 6s onwards, h=2500 W/(m^2·K)

Fluent simulations by Fortum were done by using ANSYS Fluent version 16.1. [31] Geometry was done in 2-D, height being 5cm and width 15cm. Model was meshed into 30 000 square cells. The energy equation was solved by using second-order central-difference for the space derivative and implicit method was used for time derivative. Time step was set to be 0.01 seconds and there were 25 iterations on each time step. General picture of the model with material properties and measure points is found in Figure 10.

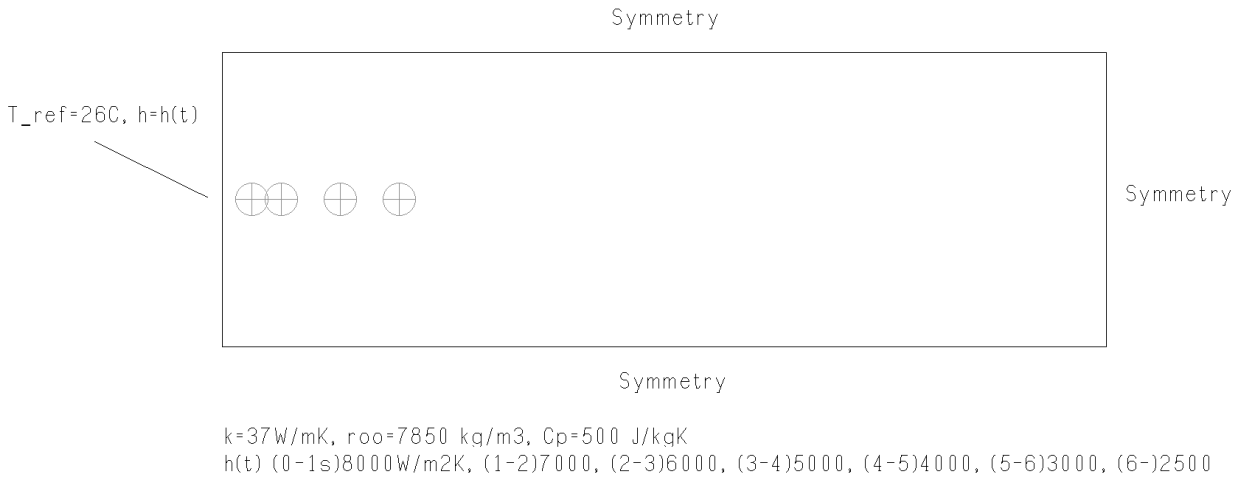

Figure 10. Created model geometry in ANSYS Fluent.

Matlab script performed excellently well. Temperature distributions on calculated measure points were almost identical. The Matlab script gave slightly higher values for all temperature distributions except at the point 30mm from surface where temperature value was slightly lower. The error in distributions averaged to less than 1 °C. ANSYS Fluent simulation results and Matlab results are compared in Figure 11.

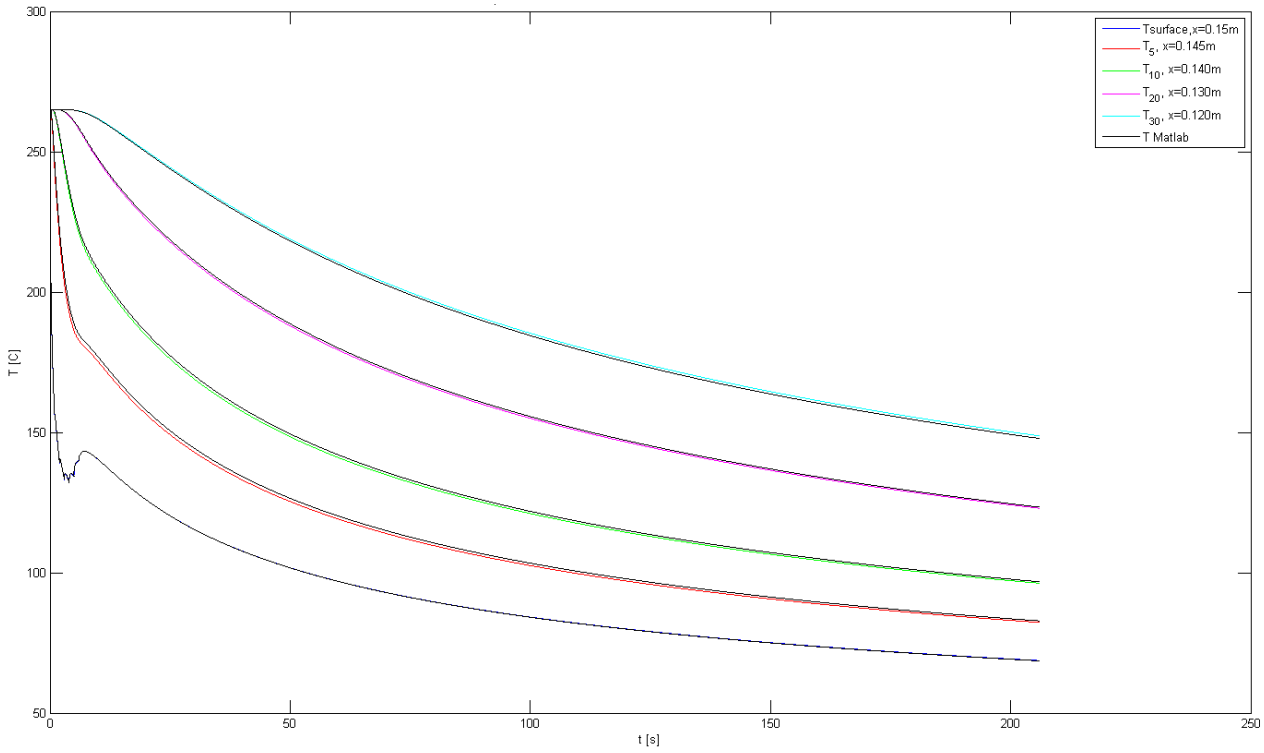

Figure 11. Comparison of the simulated results.

4.4.2 Validation by experimental data

Some of the experimental data from heat transfer experiments performed at LUT were used for validation. Heat transfer experimentations and results are documented throughout and they are found in reference [25]. Four different cases of heat transfer experiments for external cooling were chosen and used for validation of the Matlab script. The initial values for experimental test cases 06, 07, 08 and 15 are listed in Table 8.

Table 8. Initial values for the test cases used in validation. [25]

Parameter	case 06	case 07	case 08	case 15
Surface temperature [°C]	258	257	257	258
Water inlet temperature [°C]	29	53	79	29
Flow rate [l/s]	1.2	2.37	2.37	2.4
Experimental time [s]	85	84	205	3611

In the validation process, the selected measure points for temperature comparison were dominated by locations used in the experiments: surface, 5, 15 and 35mm from surface. In all the Matlab models the starting homogeneous temperature for geometry was nominated by the test case's surface temperature. In the carried out experiments the temperatures were not homogenous, they slightly increased in depth. Temperature at the depth of 35mm was overall few Celsius higher than elsewhere. The slightly higher temperature was not taken into consideration when Matlab model was validated. Calculated Matlab results with comparison to all individual cases are found in the Figures 12-15.

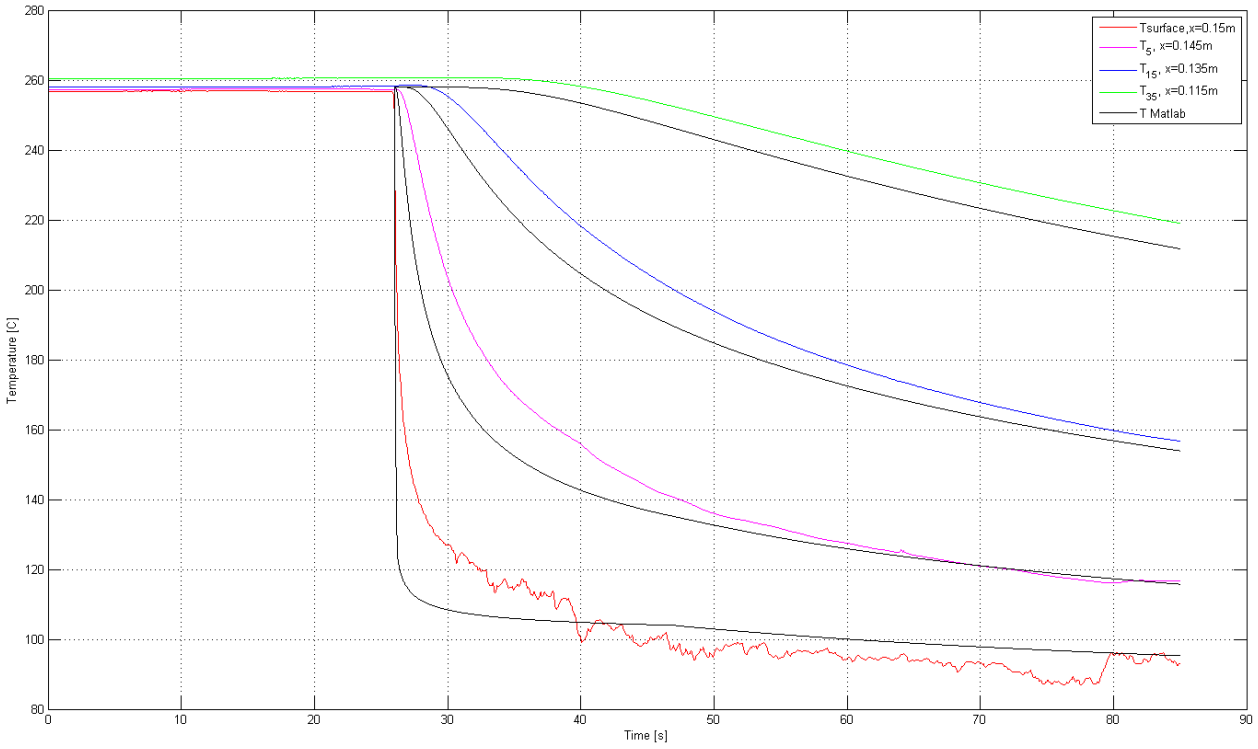

Figure 12. Test case 06, lower flow rate.

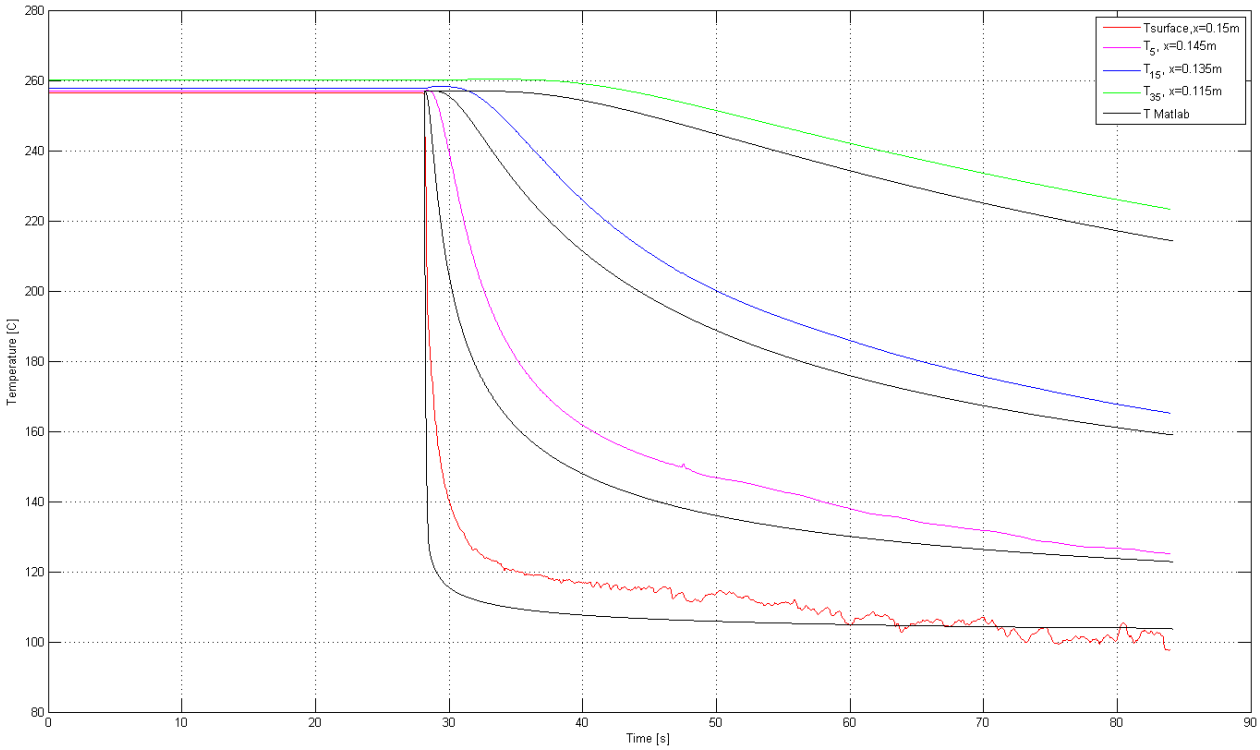

Figure 13. Test case 07, water inlet temperature 53 Celsius.

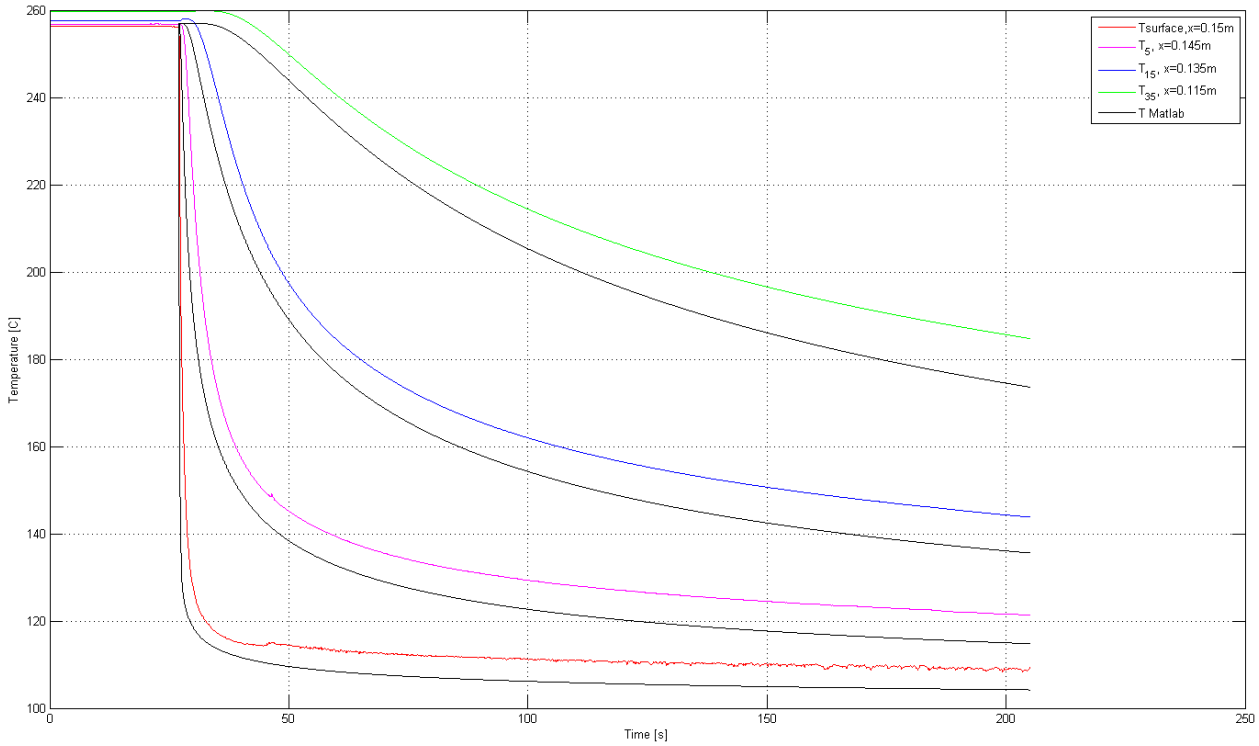

Figure 14. Test case 08, water inlet temperature 79 Celsius.

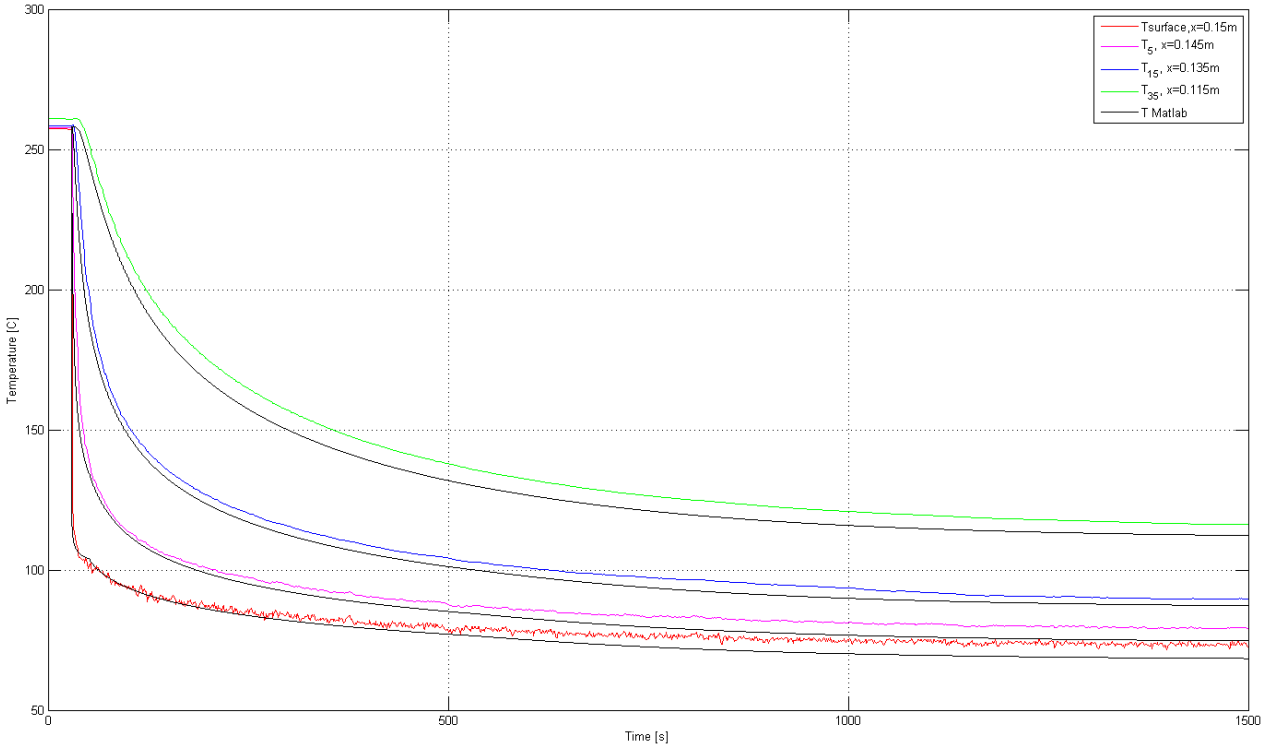

Figure 15. Test case 15, steady state calculations.

In most of the cases the temperature distributions calculated by Matlab script are dropping more sharply than in the compared experimental cases. The sharp drop in Matlab script is caused by the assumption explained section 4.1.2, the CHF is assumed when the surface temperature is above 130 Celsius. The first few seconds of strong heat transfer is causing biggest stresses within the RPV. The sharper drop in temperature distributions within the first few seconds is conservative in the case where the goal is to mitigate the temperature drop.

The overall accuracy in all of the validation cases is satisfactory. Test case 15 gave the best results. The reason for this is most likely Equation 13. The correlation made by Fortum for post boiling was engineered from the test case 15.

4.5 Test facility in LUT

The main component in the test facility is low alloy steel bar 10CrMo9-10 that has approximately same wall thickness as the RPV used in Loviisa, 150mm. The bar is long enough for observation of vertical phenomenon in the flow channel. In addition the heat transfer properties are close to the steel used in Loviisa RPV. The steel bar has a heater on

one side and is enclosed in flow channel on the other side. The heater element contains six rods that contribute the total power of 6kW. [25]

The width of the flow channel is 100mm and the length is 300mm. For achieving constant velocity distribution, the flow channel is connected to pipeline that has expansion at the inlet and reduction at the outlet. The original test facility had two windows for visual observation purposes. The current test facility has two additional windows for allowing the use of particle image velocimetry (PIV). [25] The current state of the test facility is presented in Figure 16.

Figure 16. The current state of the test facility

Temperature measurement has total of 34 K-type thermocouples with 3mm or 1mm outer diameter. Four 1mm thermocouples are installed on the surface of the steel bar. 26 of the thermocouples are divided into four rows and they are measuring temperature within the steel bar, 6 are measuring water temperatures in the flow channel and 2 are measuring temperatures from the flow channel inlet and flow meter. The exact locations for thermocouples in single row are: surface, 5mm, 15mm, 35mm, 70mm and 110mm from

the surface. The flow chart and the locations of thermocouples are illustrated in Figure 17. [25]

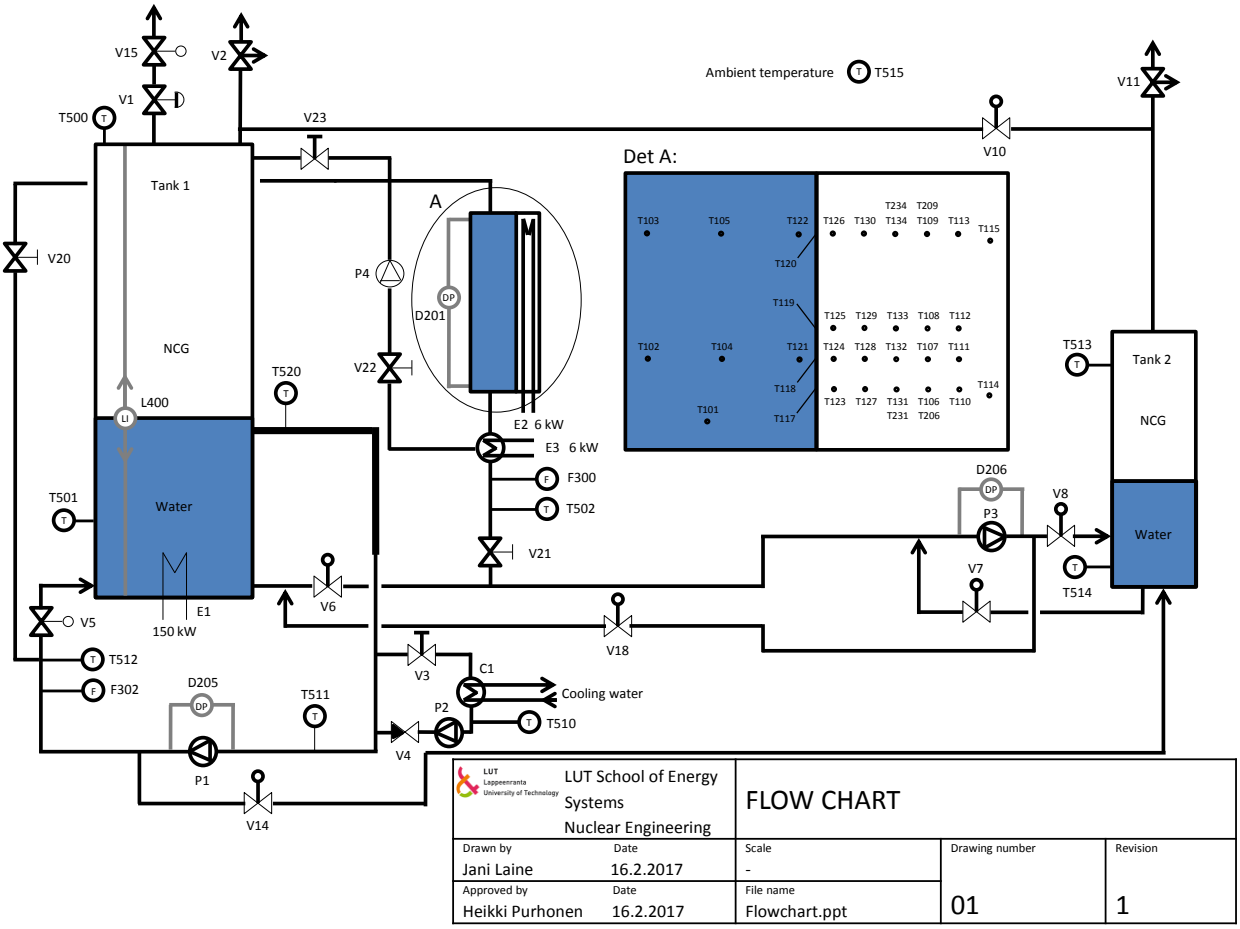

Figure 17. Flow chart of the test facility.

In 2008, heat transfer experiments for external cooling were performed with the test facility. These experiments included surface temperature measurements, estimations of heat fluxes and heat transfer coefficient and steady state experiments. The main parameters that were varied in the test series were: flow rate, water inlet temperature and the steel bar temperature.

5 TEMPERATURE DISTRIBUTION RESULTS

The starting values for external cooling calculations were taken from the postulated external cooling sequence (section 2.3). The minimum water temperature in the gap between RPV and concrete wall was estimated to be 37 °C during the case. [13] This temperature value was set to be constant during the whole calculation progress. The RPV thickness was set to be 149mm with uniform temperature of 266 °C at the beginning of the transient. In all cases, the temperatures are calculated at surface, 5mm, 15mm and 35mm from the RPV surface to inwards. In addition to the cases, where the added insulation thickness is more than 5mm, additional temperature distribution is calculated at 5mm from the RPV surface within the insulation. The most stress to RPV integrity during cooling happens within the first few seconds. The overall simulation time was set to be 200 seconds so it definitely includes the alleged thermal shock.

Using the Equation 2, the Unit thermal resistances of the insulation materials with varying thicknesses are illustrated in Figure 18. Calcium silicate and macor appear to be the best insulators.

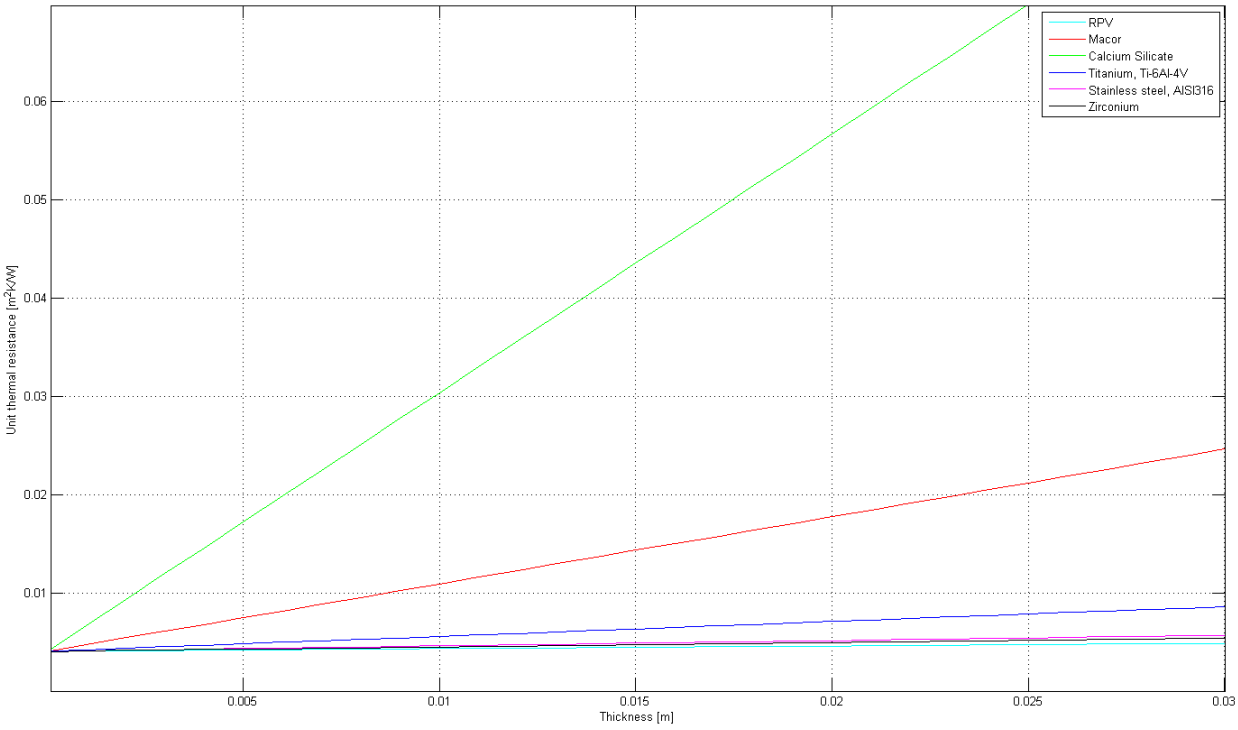

Figure 18. Unit thermal resistance in respect to different thicknesses added to existing RPV thickness.

5.1 RPV without thermal insulation

The postulated external cooling transient was calculated without any thermal insulation. Temperature distribution in the whole RPV is displayed in Figure 19. Calculated heat transfer coefficient is found in Figure 20. Temperature distributions are illustrated in Figure 21.

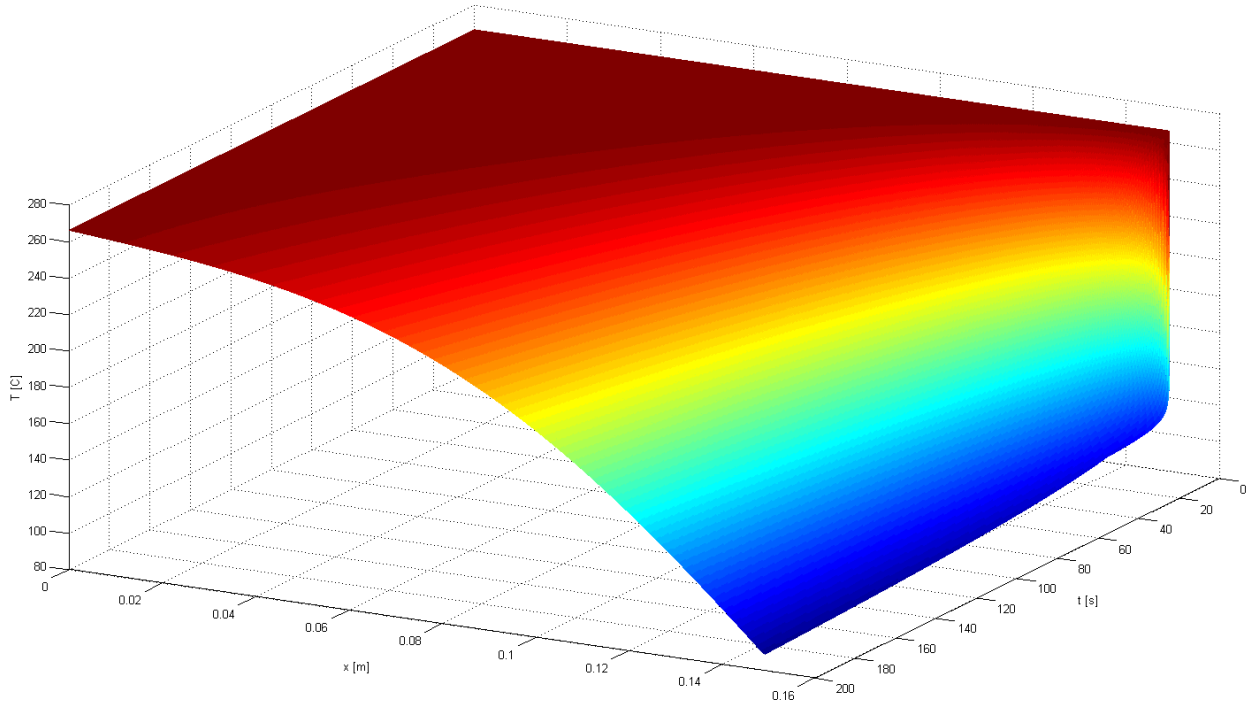

Figure 19. Complete temperature distribution within the RPV.

As expected, the surface temperature drops rapidly with the heat transfer coefficient correlation giving values that are reaching CHF. Momentarily the heat transfer coefficient (Figure 20) is twice larger than the heat transfer coefficient calculated by APROS for the similar case (see Figure 6).

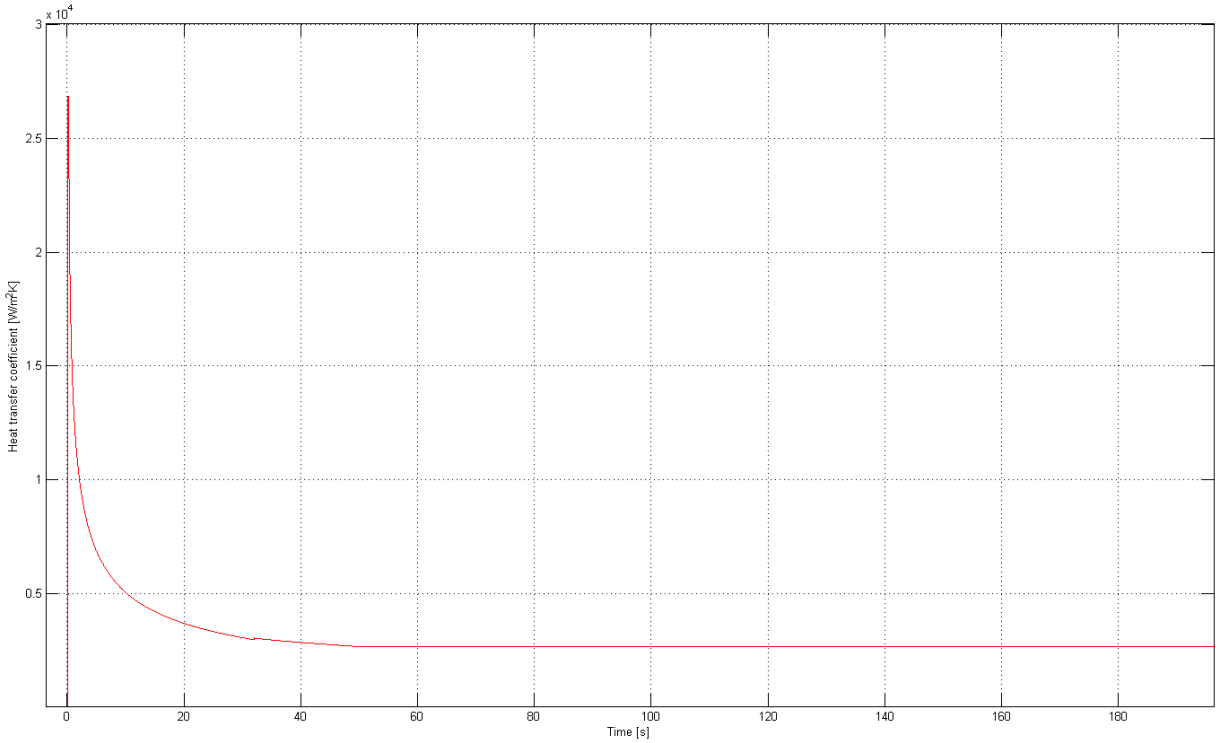

Figure 20. Calculated heat transfer coefficient from the RPV surface to water.

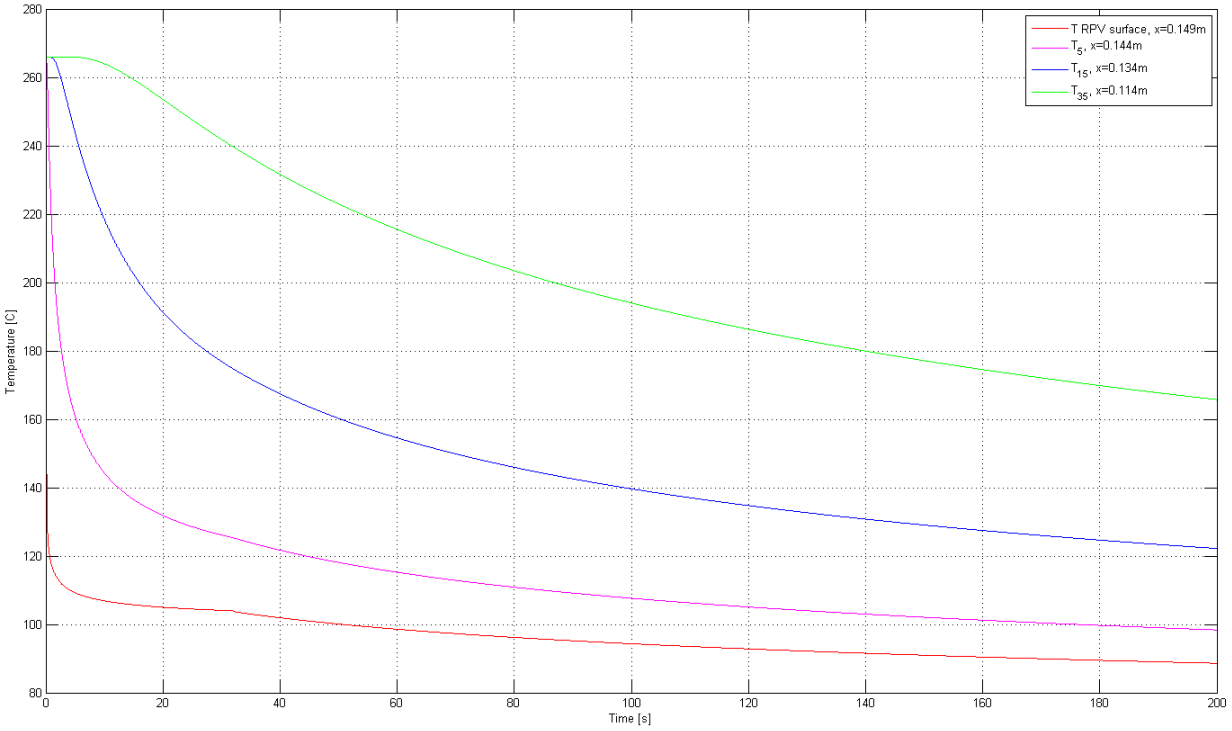

Figure 21. Temperature distribution within the RPV.

5.2 Macor

Temperature distributions were calculated for four different thicknesses of macor. The simulations were performed for the thicknesses of 3mm, 5mm, 1cm and 2cm. The corresponding temperature distribution results are shown in Figures 22-25. The 3D distribution for 3mm thickness is found in Figure 26. The 3D graph illustrates the overall impact of thermal insulation very effectively.

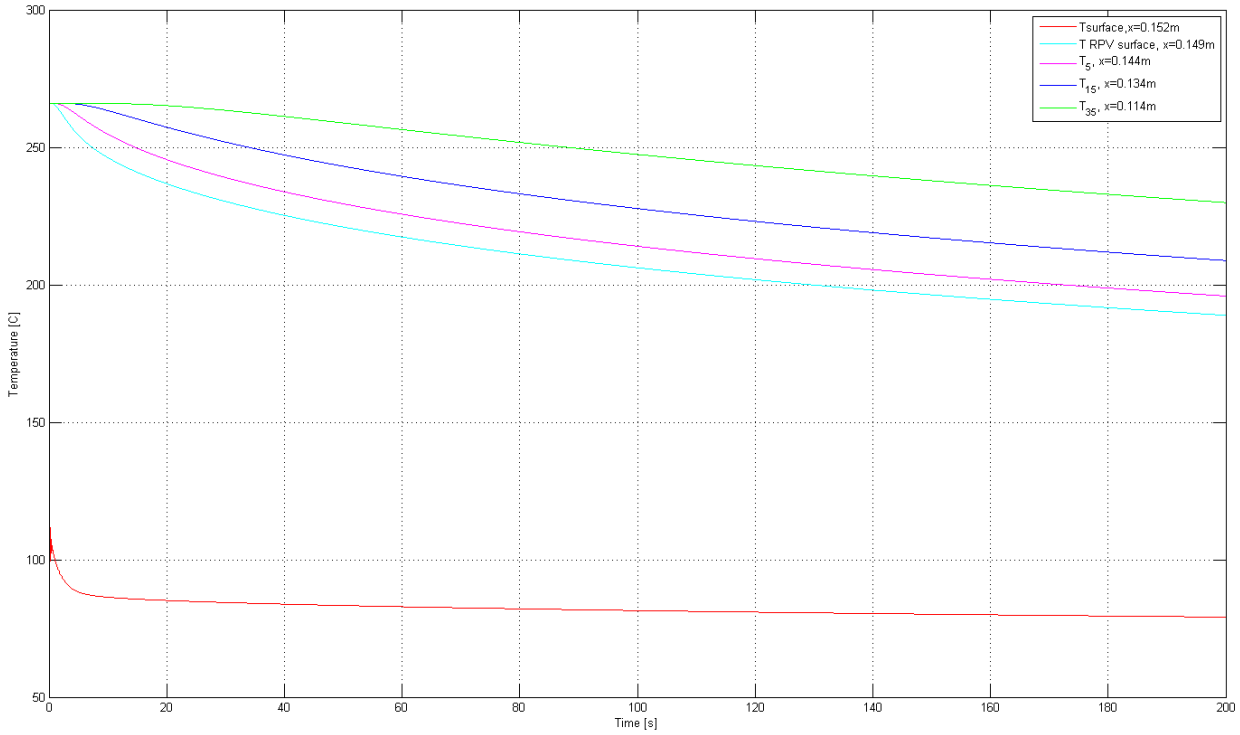

Figure 22. Temperature distribution within the RPV wall with 3 mm thick thermal insulation layer of macor.

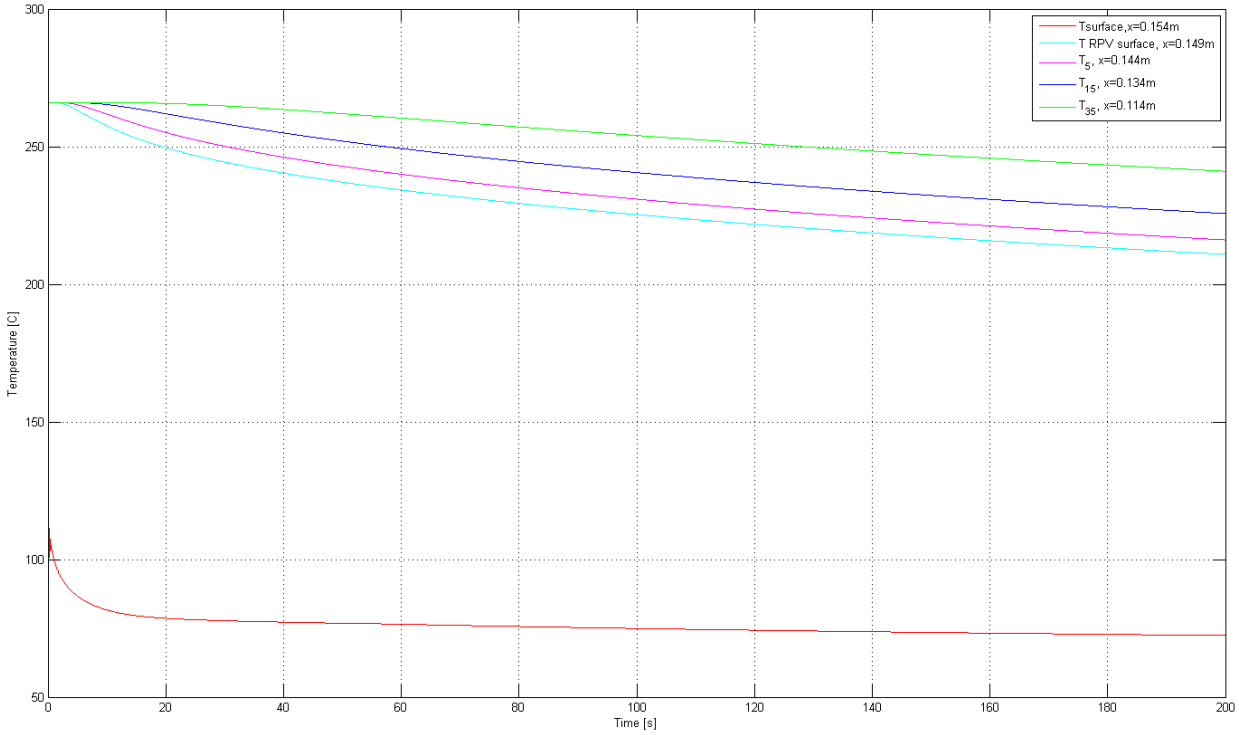

Figure 23. Temperature distribution within the RPV wall with 5 mm thick thermal insulation layer of macor.

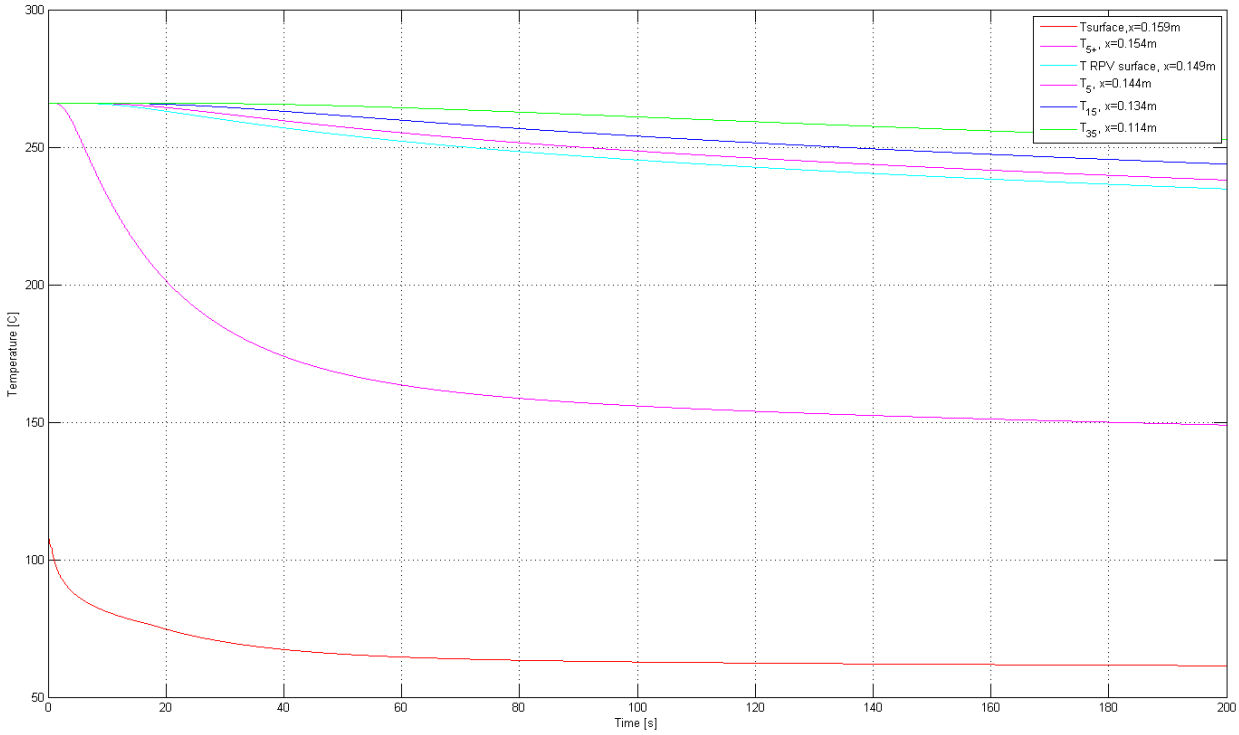

Figure 24. Temperature distribution within the RPV wall with 1 cm thick thermal insulation layer of macor.

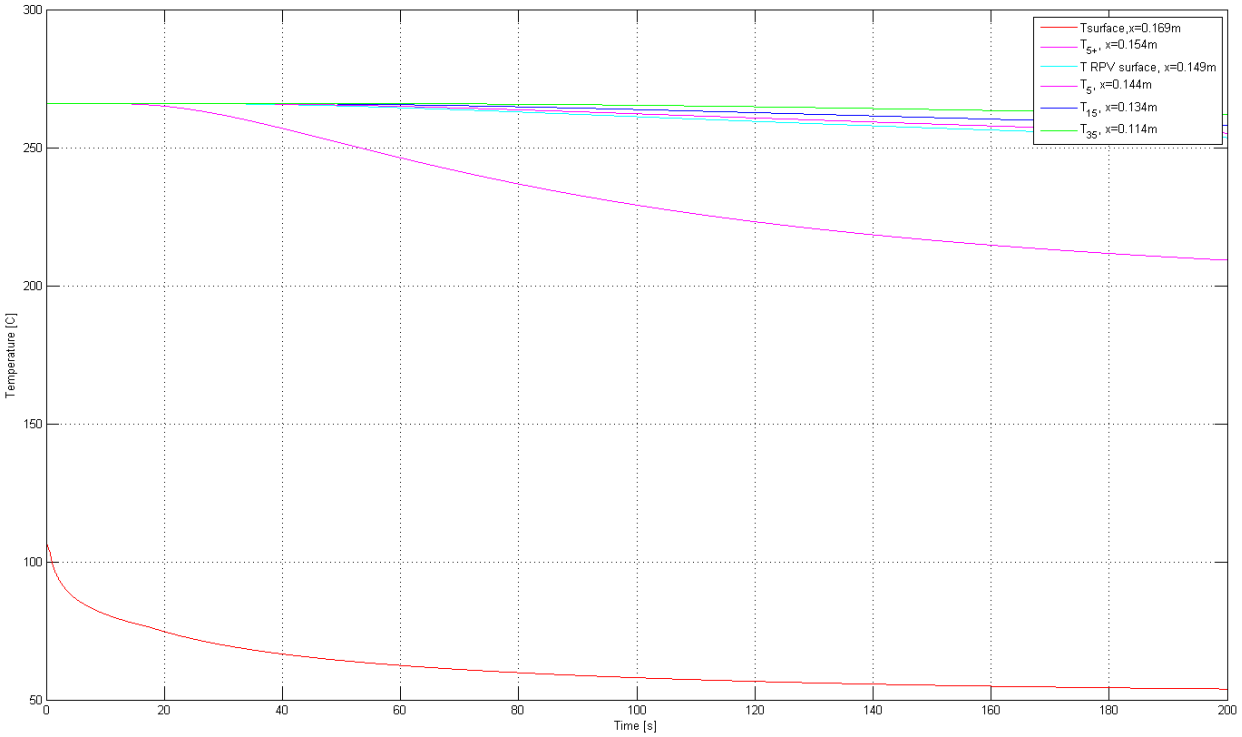

Figure 25. Temperature distribution within the RPV wall with 2cm thick thermal insulation layer of macor.

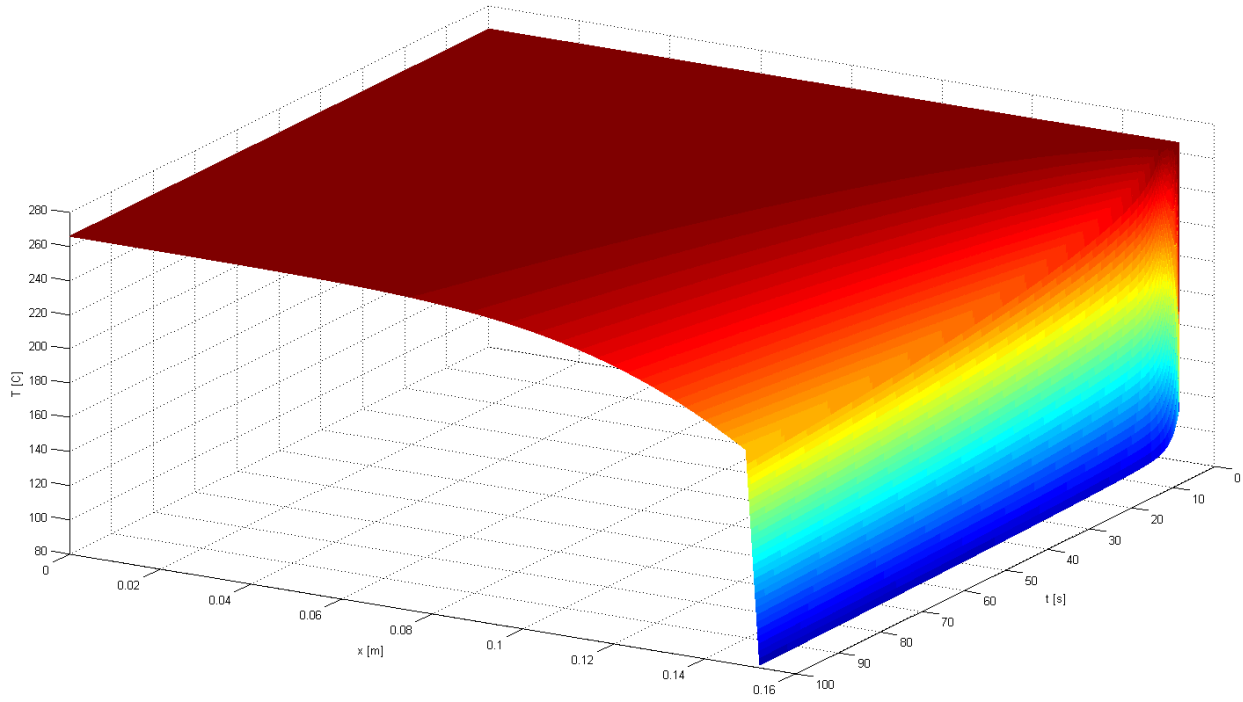

Figure 26. Complete temperature distribution with 3mm thick thermal insulation layer of macor.

5.3 Calcium silicate

Temperature distributions for calcium silicate were calculated for thicknesses of 3mm, 5mm and 1cm. Out of the selected insulation materials, the unit thermal resistance is the highest when calcium silicate is applied. This can be seen the surface temperature of RPV being very high in Figures 27-29.

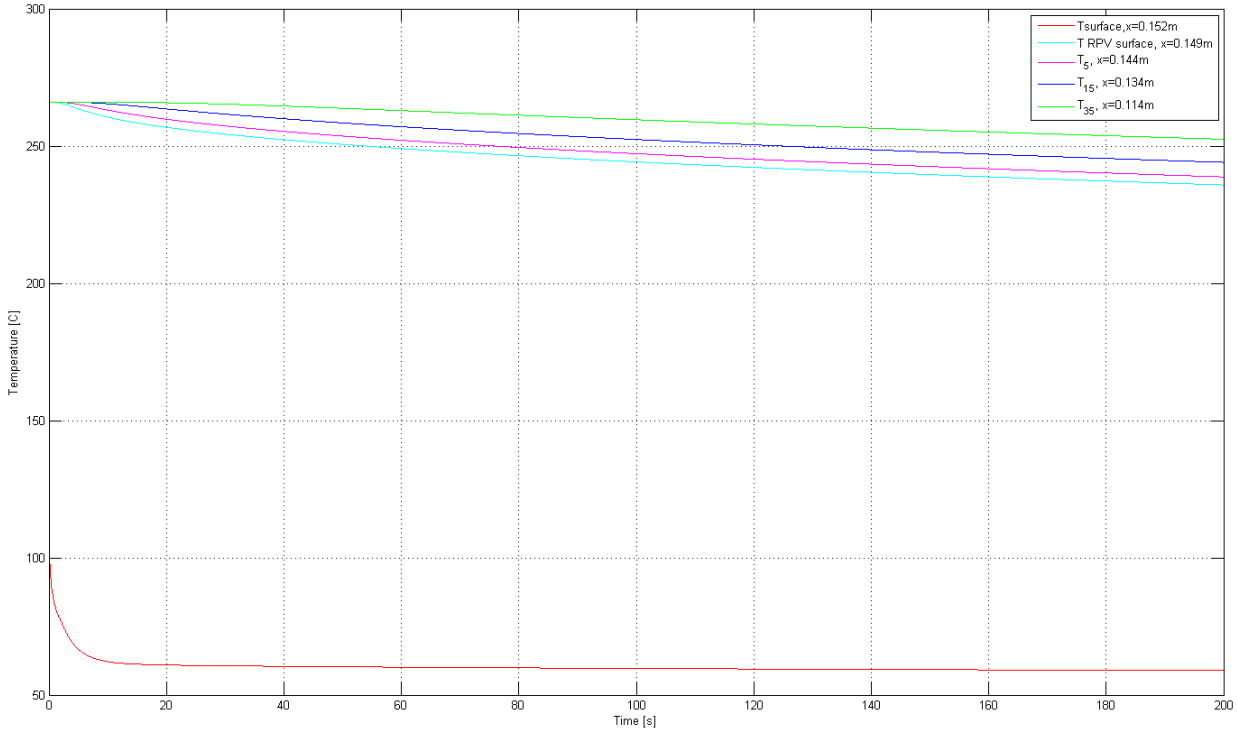

Figure 27. Temperature distribution within the RPV wall with 3mm thick thermal insulation layer of calcium silicate.

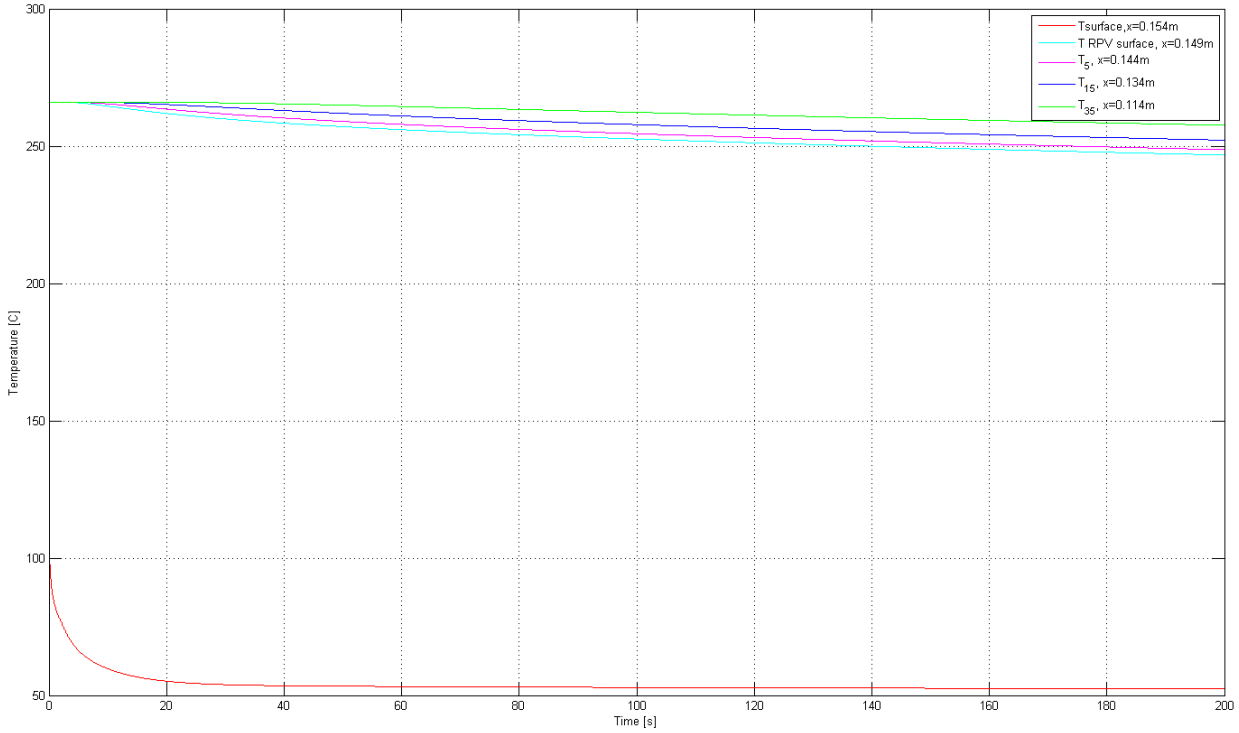

Figure 28. Temperature distribution within the RPV wall with 5mm thick thermal insulation layer of calcium silicate.

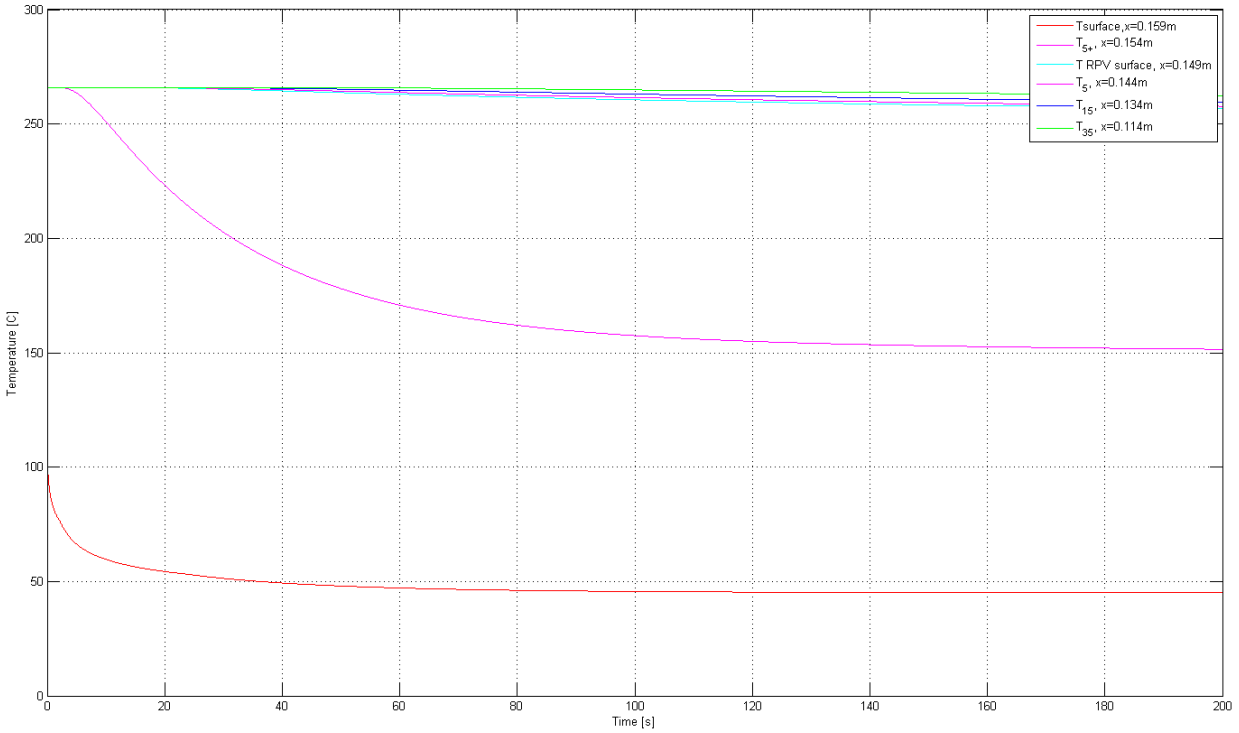

Kuva 29. Temperature distribution within the RPV wall with 1cm thick thermal insulation layer of calcium silicate.

5.4 Stainless steel AISI316

Stainless steel AISI316 has similar properties with the RPV. Calculations were performed for the thicknesses of 5mm, 1cm, 2cm and 3cm. Results for the temperature distributions are found in Figures 30-33. When the thickness of AISI316 exceeds 1cm, the mitigation effect improves. This can be clearly seen when comparing Figures 31 and 32.

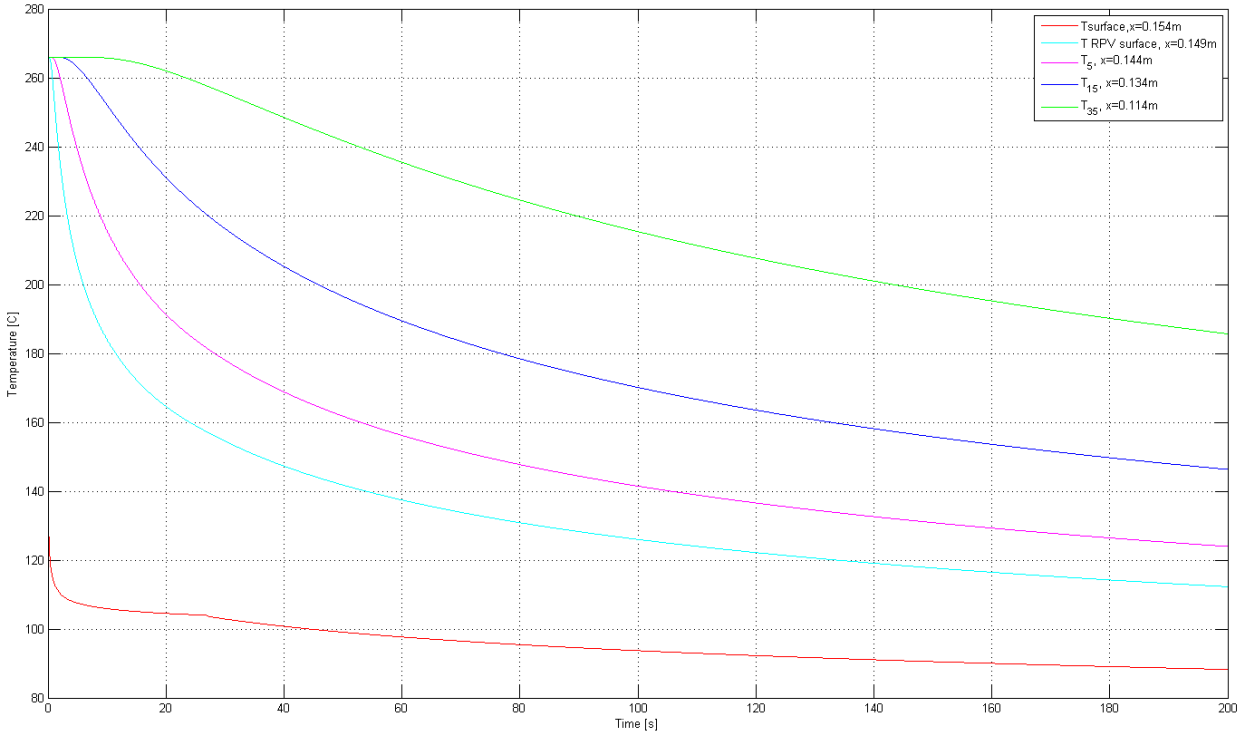

Figure 30. Temperature distribution within the RPV wall with 5mm thick thermal insulation layer of AISI316.

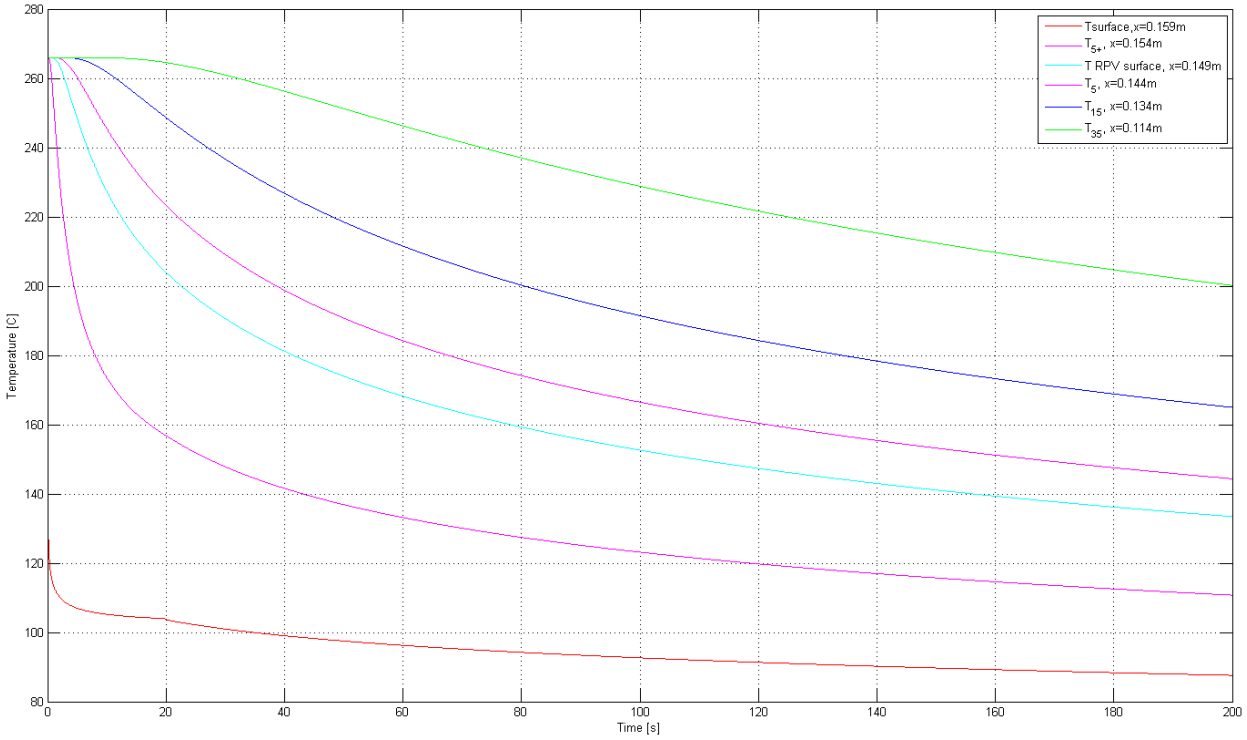

Figure 31. Temperature distribution within the RPV wall with 1cm thick thermal insulation layer of AISI316.

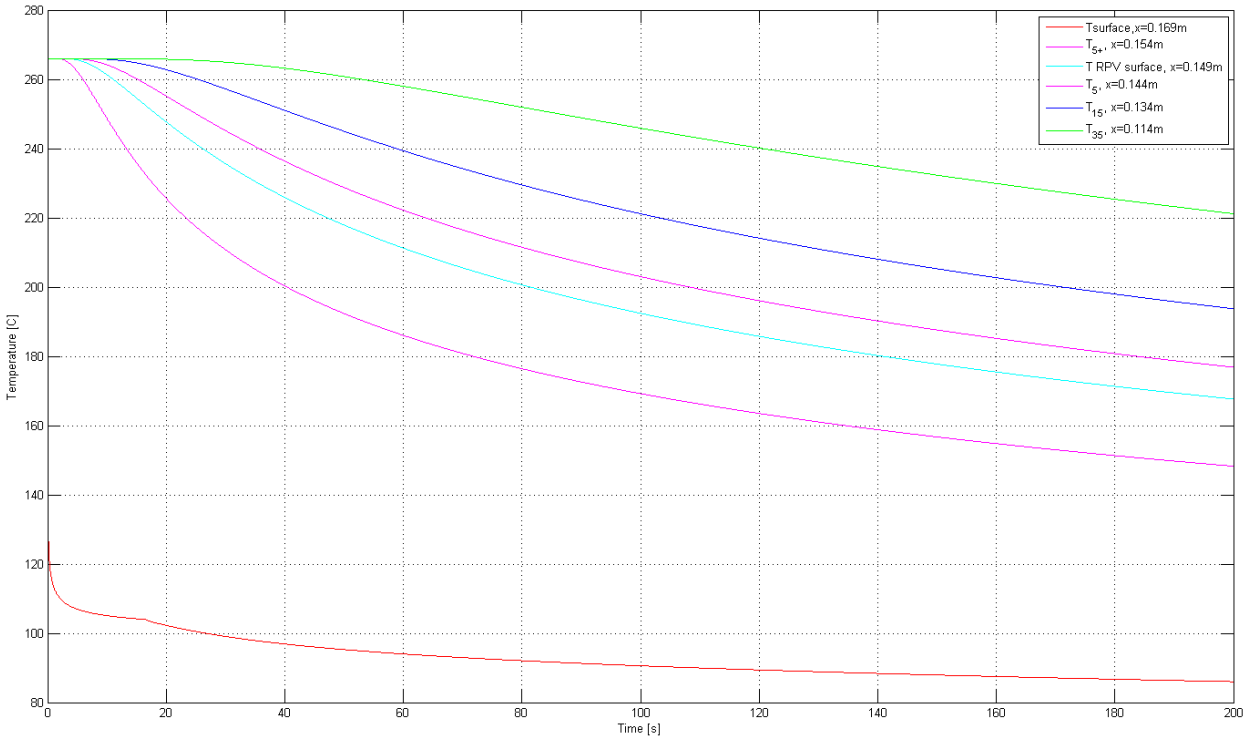

Figure 32. Temperature distribution within the RPV wall with 2cm thick thermal insulation layer of AISI316.

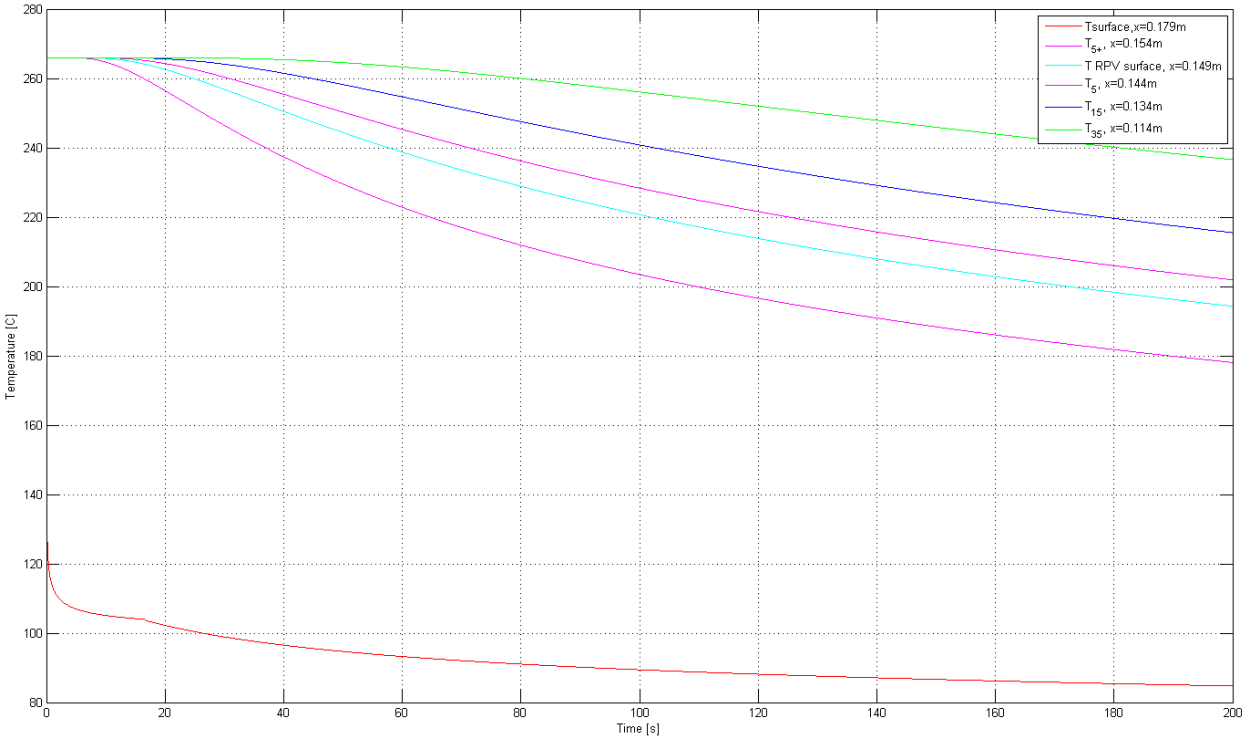

Figure 33. Temperature distribution within the RPV wall with 3cm thick thermal insulation layer of AISI316.

5.5 Titanium Ti-6Al-4V

Titanium Ti-6Al-4V has the best thermal properties out of the selected metals. Calculations were performed for the thicknesses of 5mm, 1cm, 2cm and 3cm. Results for the temperature distributions are found in Figures 34-37. The mitigation effect already improves when the thickness is above 5mm.

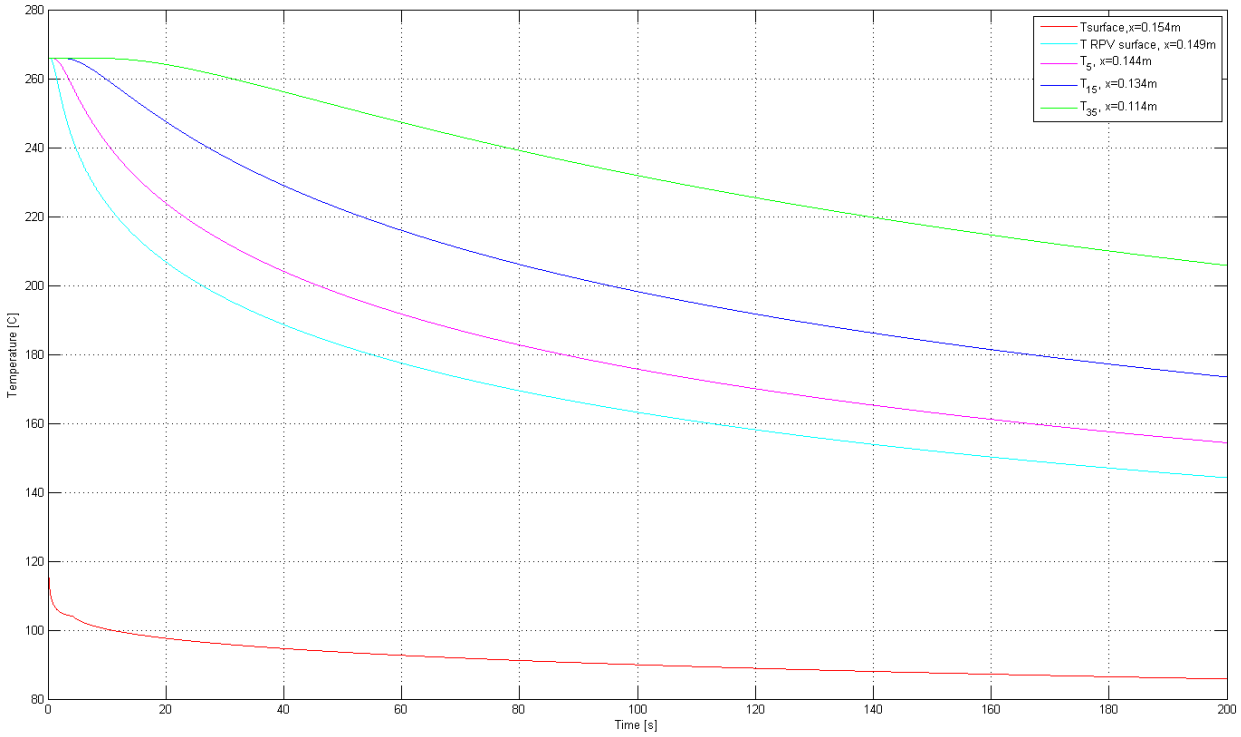

Figure 34. Temperature distribution within the RPV wall with 5mm thick thermal insulation layer of Ti-6Al-4V.

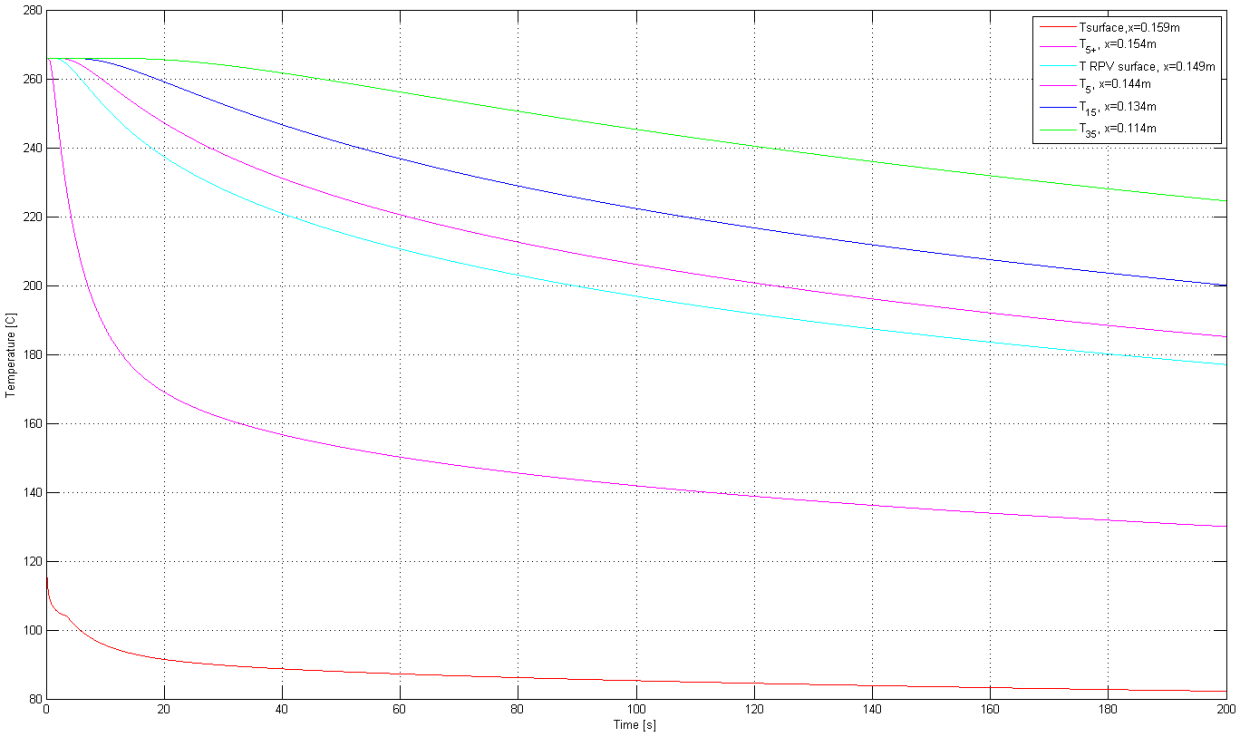

Figure 35. Temperature distribution within the RPV wall with 1cm thick thermal insulation layer of Ti-6Al-4V.

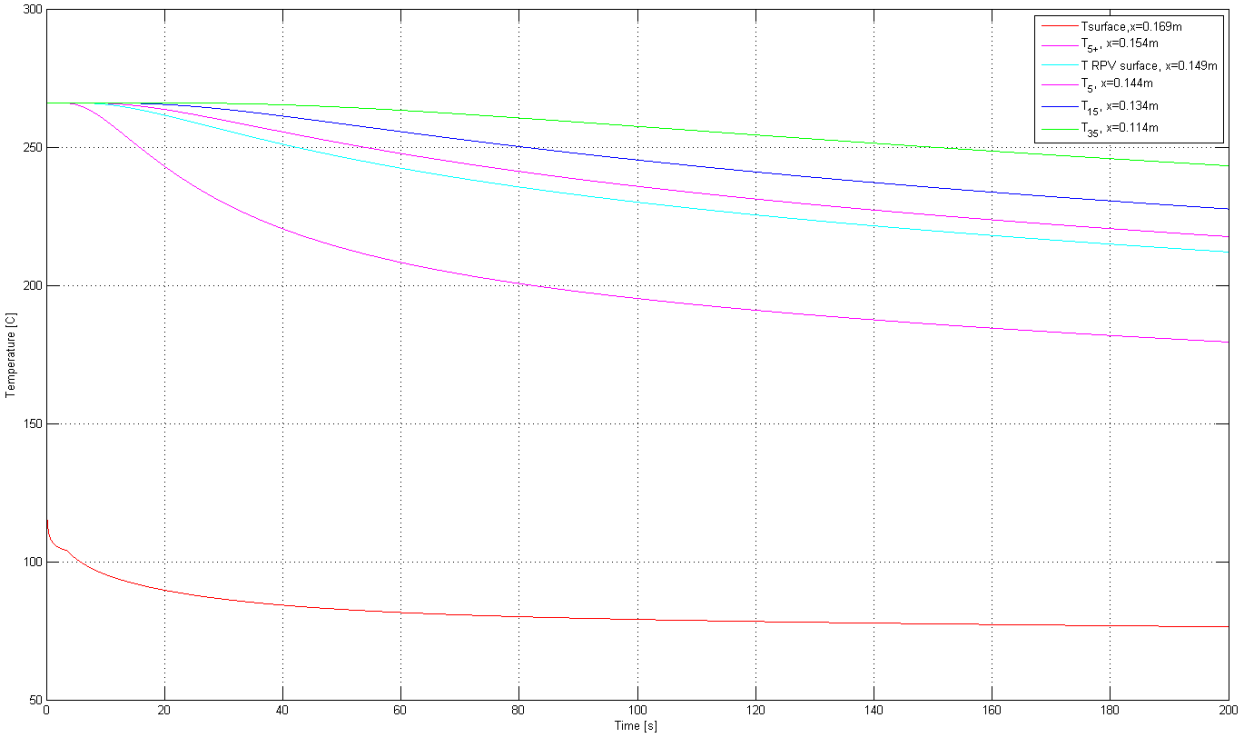

Figure 36. Temperature distribution within the RPV wall with 2cm thick thermal insulation layer of Ti-6Al-4V.

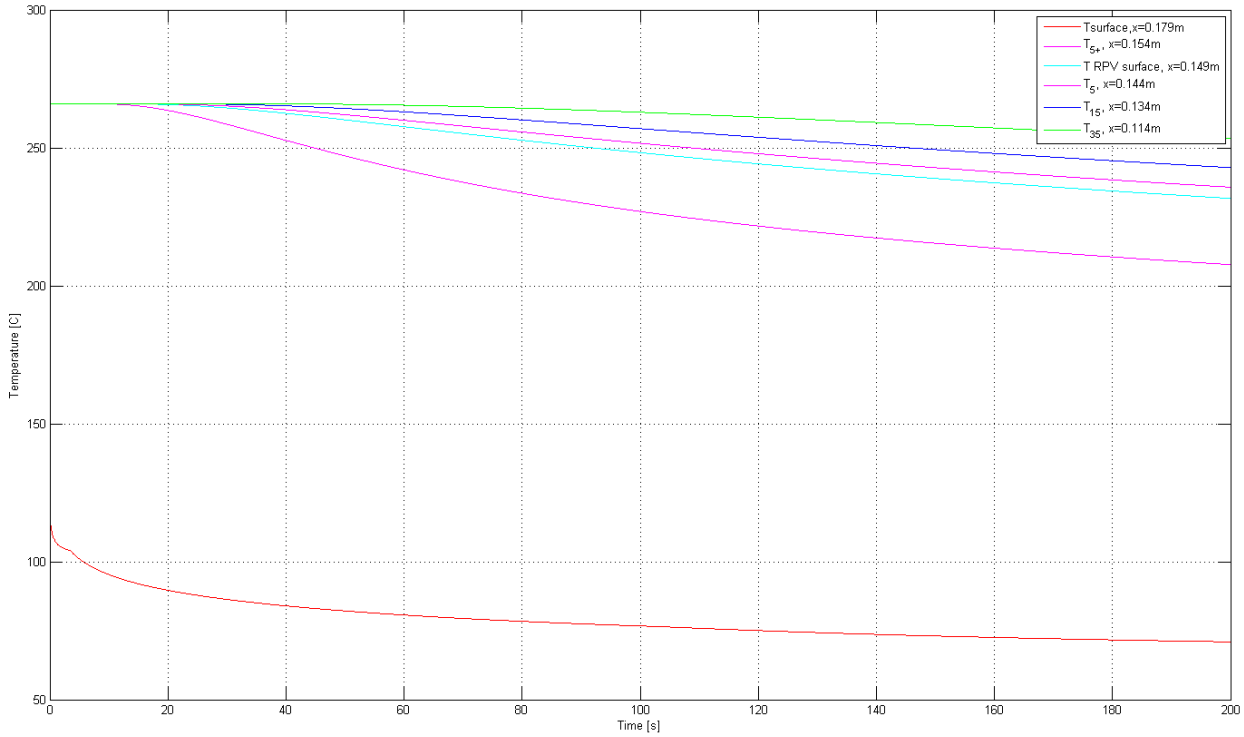

Figure 37. Temperature distribution within the RPV wall with 3cm thick thermal insulation layer of Ti-6Al-4V.

5.6 Zirconium

Out of the chosen materials, zirconium had the highest thermal conductivity. Calculations were performed for the thicknesses of 5mm, 1cm, 2cm and 3cm. Temperature distributions are found in Figures 38-41. The similar mitigation to other chosen metals is achieved when the thickness for zirconium exceeds 2cm.

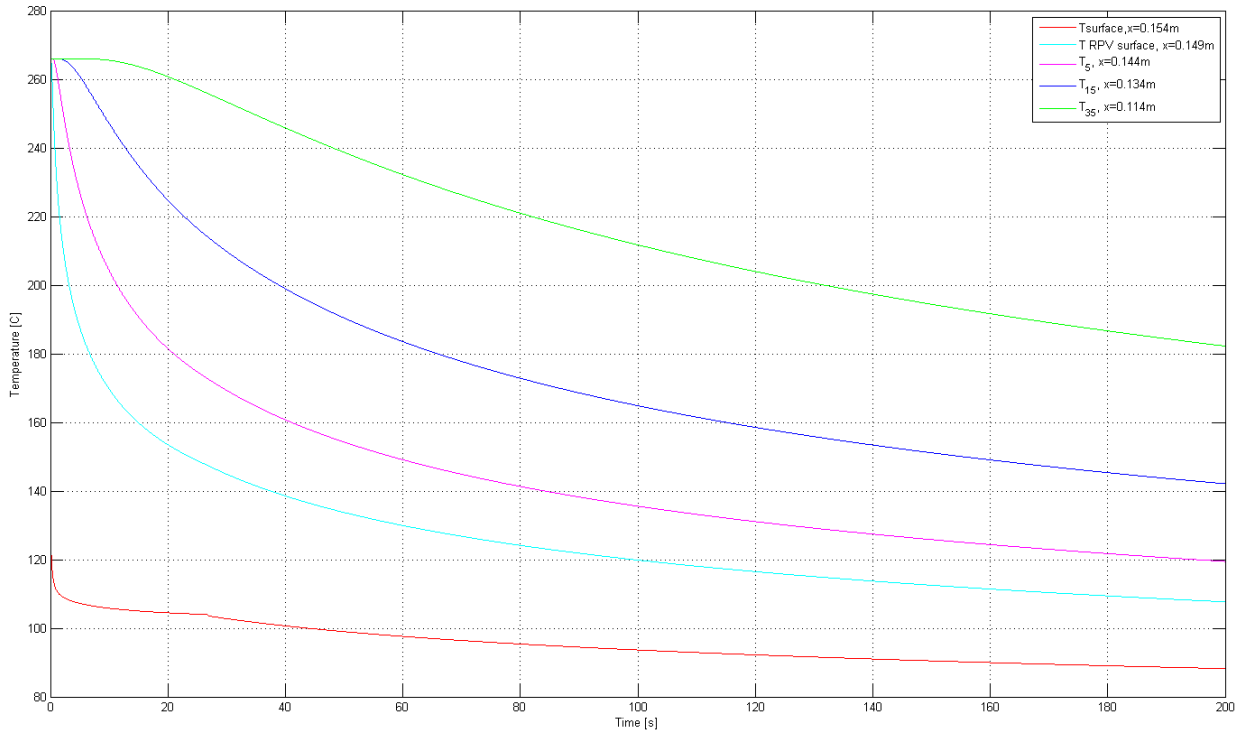

Figure 38. Temperature distribution within the RPV wall with 5mm thick thermal insulation layer of zirconium.

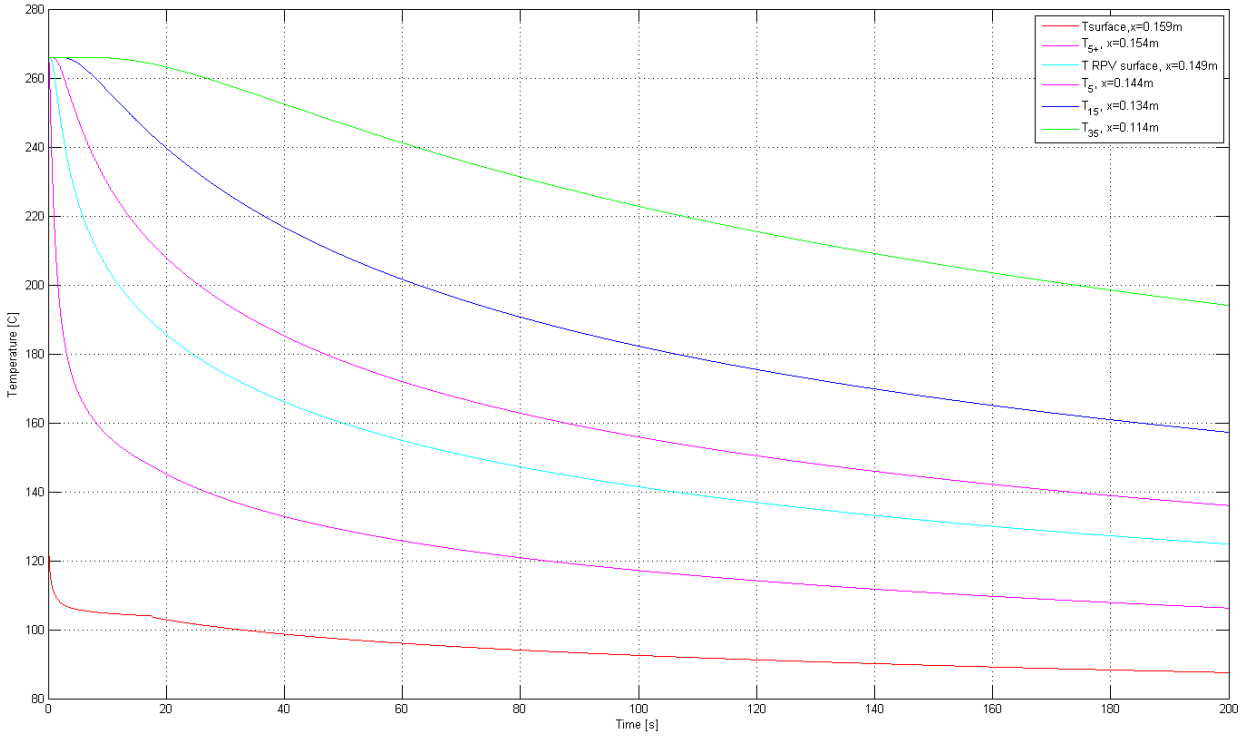

Figure 39. Temperature distribution within the RPV wall with 1cm thick thermal insulation layer of zirconium.

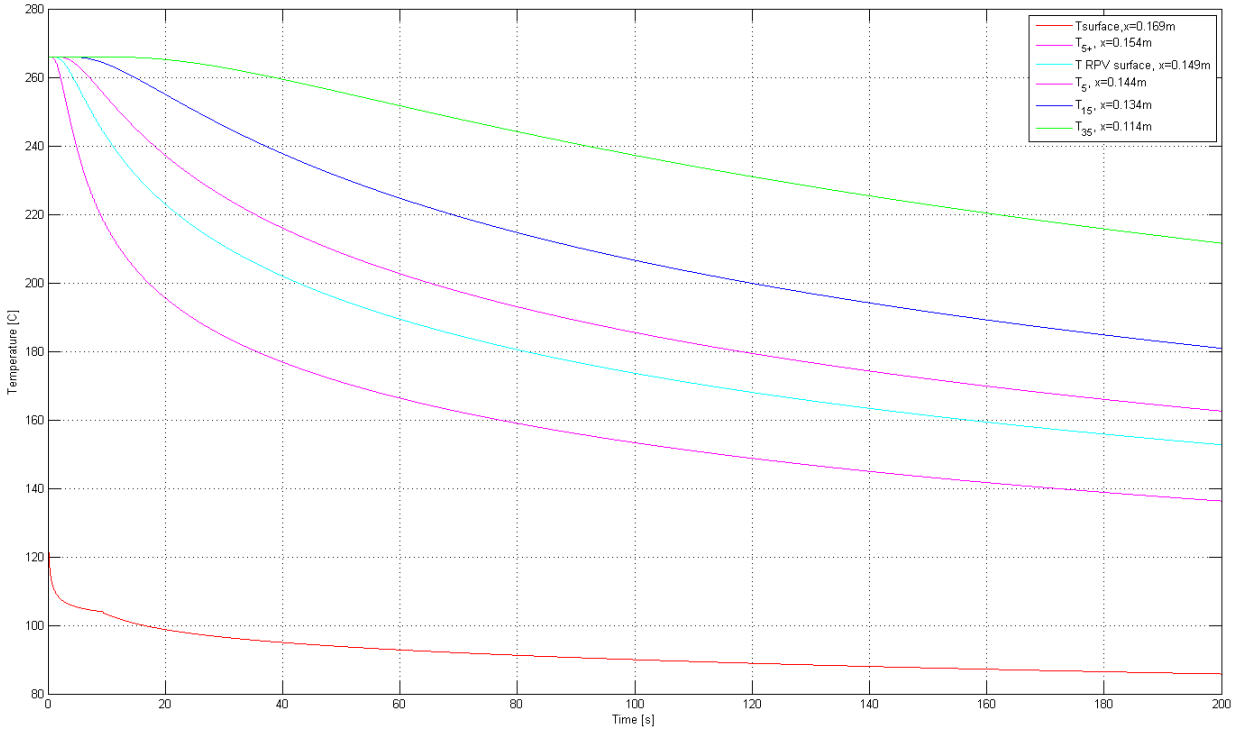

Figure 40. Temperature distribution within the RPV wall with 2cm thick thermal insulation layer of zirconium.

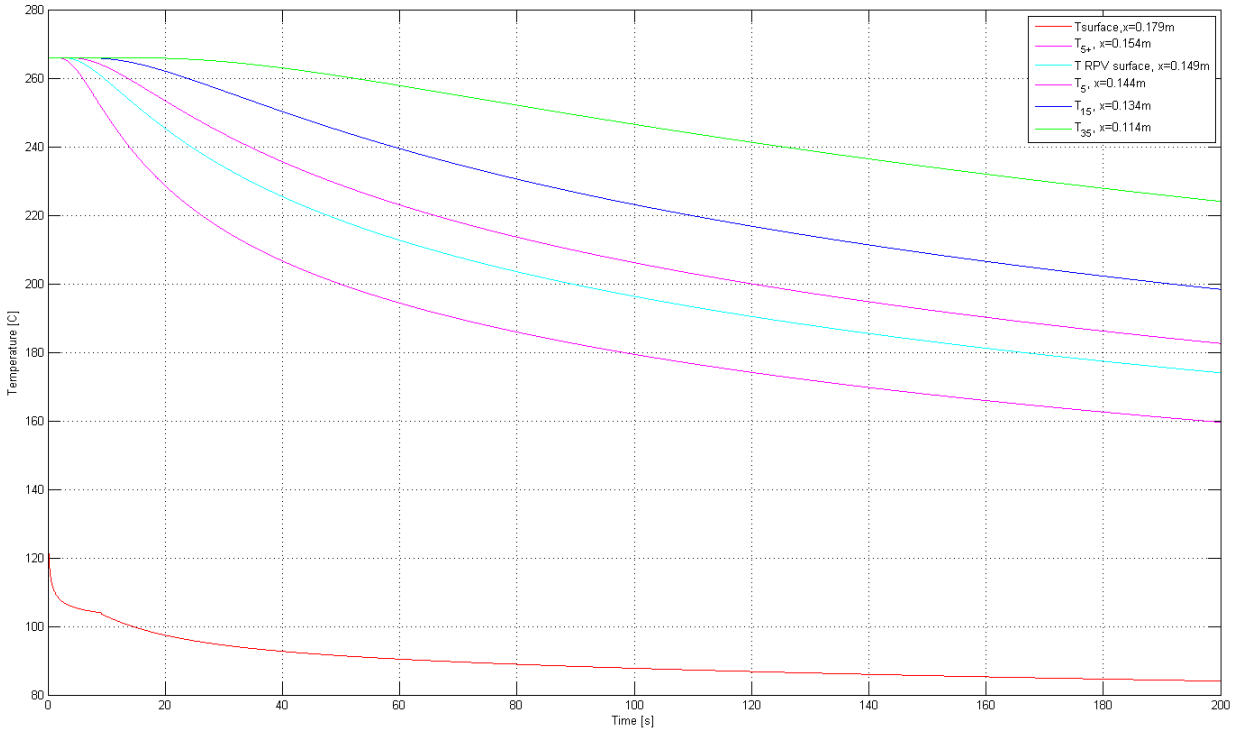

Fihure 41. Temperature distribution within the RPV wall with 3cm thick thermal insulation layer of zirconium.

5.7 Steady state distributions

Steady state calculations were used to verify validity of equation 2 and inspect that the heat flux across the whole system is equal. Temperature distributions after 4000 seconds for AISI316, zirconium and Ti-6Al-4V are found in Figures 42-44. The steady state was not completely reached even after 4000 seconds. Table 9 contains the calculated values for heat fluxes across the system.

Table 9. Approximate heat fluxes across the system after 4000seconds of simulation.

Material	**q_x through RPV**	**q_x through insulation**	**q_x from surface to water**
AISI316	35 kW/m^2	34.8 kW/m^2	36.3 kW/m^2
Zirconium	36.8 kW/m^2	36.6 kW/m^2	38.6 kW/m^2
Ti-6Al-4V	23.2 kW/m^2	24 kW/m^2	24.5 kW/m^2

Ti-6Al-4V being the most effective thermal insulator is plotted as 3D graph in Figure 45. Resemblance is obvious when comparing the 3D graph with Figure 7.

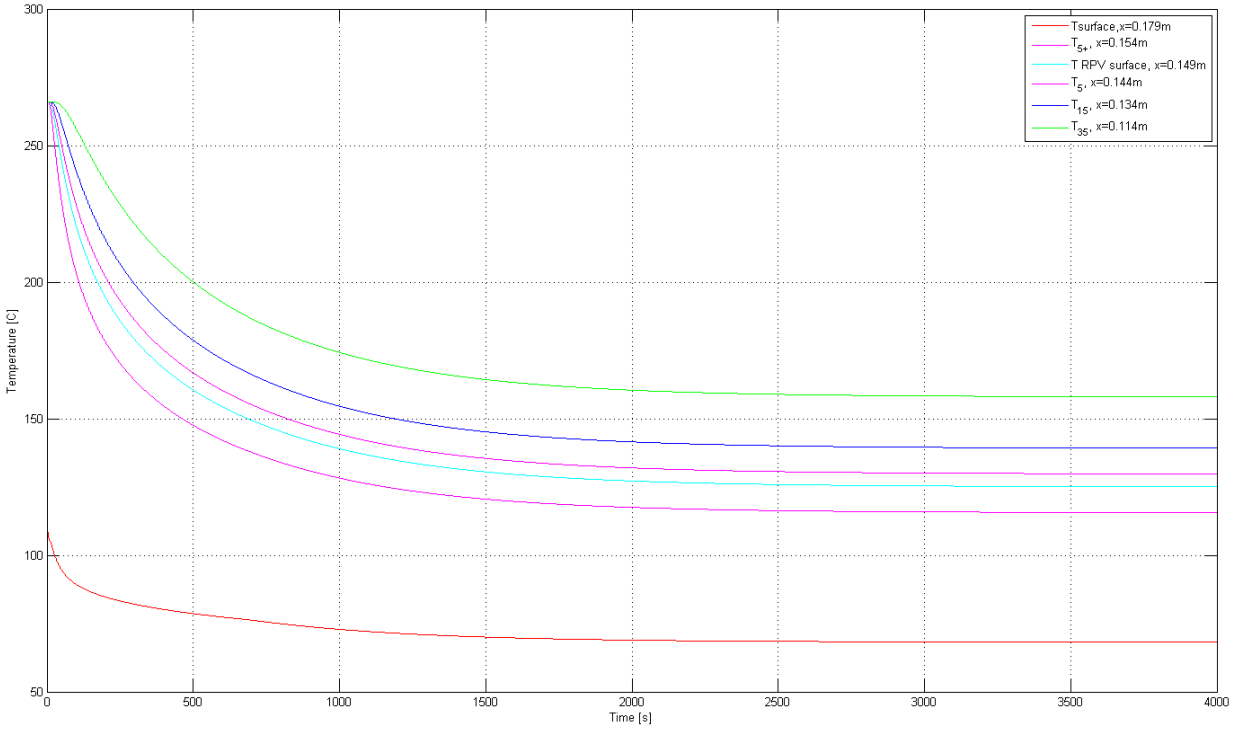

Figure 42. Temperature distribution within the RPV wall with 3cm thick thermal insulation layer of AISI316.

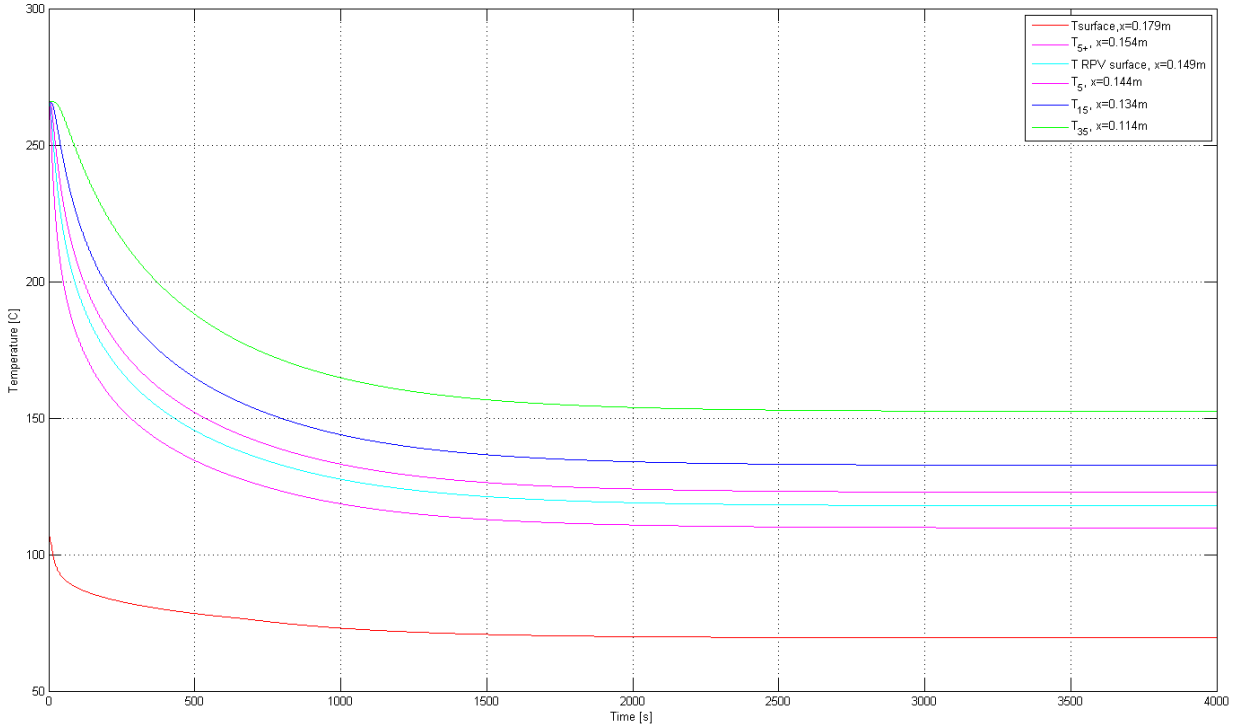

Figure 43. Temperature distribution within the RPV wall with 3cm thick thermal insulation layer of Zirconium.

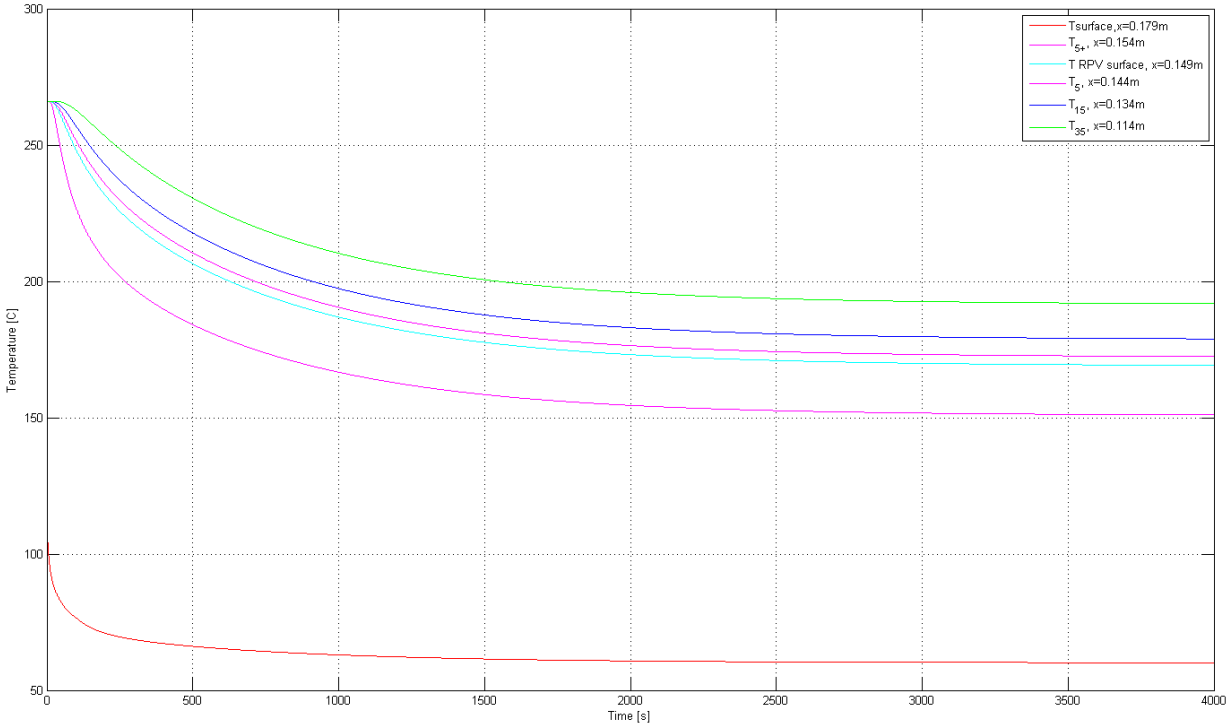

Figure 44. Temperature distribution within the RPV wall with 3cm thick thermal insulation layer of Ti-6Al-4V.

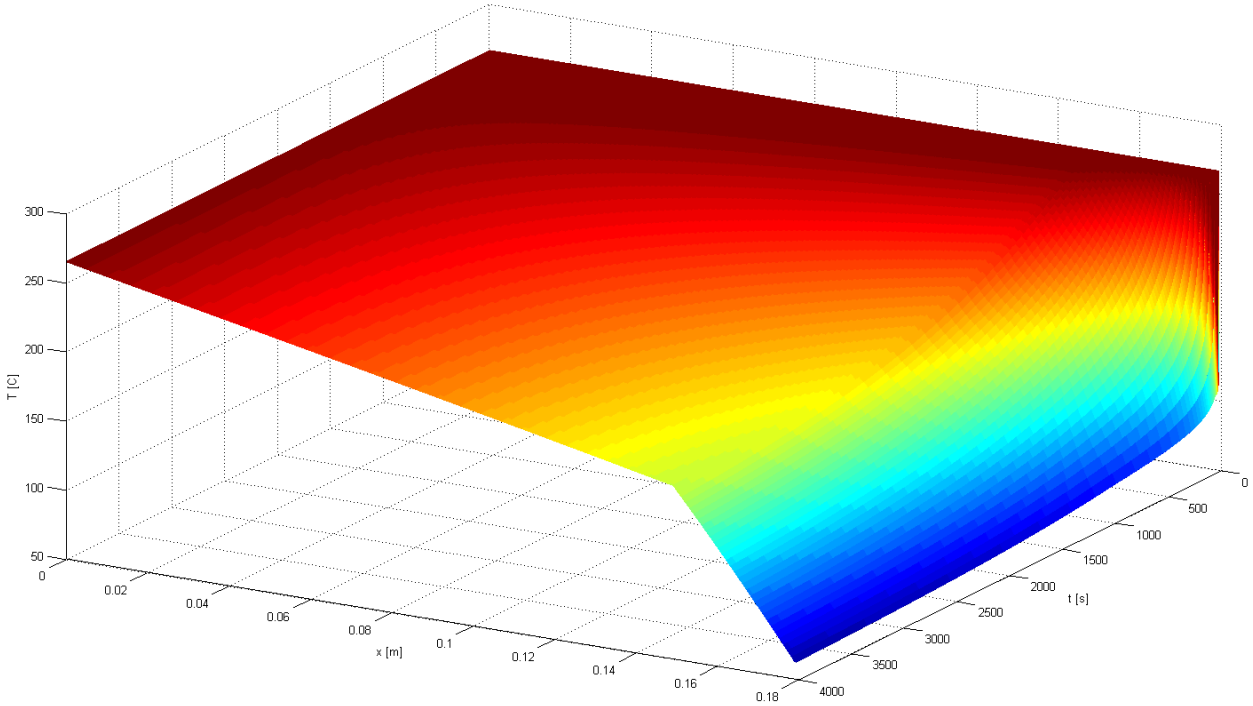

Figure 45. Complete temperature distribution with 3cm thick thermal insulation layer of Ti-6Al-4V after 4000seconds.

6 CONCLUSIONS AND FURTHER RESEARCH

Most researched thermal insulation materials were rejected due to poor radiation resistance or unsuitable temperature resistance. Among the rejected materials were PTFE, polyurethane, paints, adhesives, rubbers, and all materials with higher concentration of manganese, phosphorous, nickel, vanadium and copper and finally the materials that deform under water contact. Metal alloys indicate to have the overall best properties to withstand the challenging conditions outside of the Loviisa RPV. Strongest thermal insulation material that was simulated was calcium silicate. This raises a question if the thermal insulation effect is too strong with calcium silicate. In reality when strong thermal insulation with larger thickness, the heat transfer during cooling transient might take place at the edge between RPV wall and the insulation leading to unwanted transients. Since the calculated cases were done 1-dimensionally with ideal heat conduction, the mentioned outcome is not predictable.

The Matlab script developed in this thesis estimates the temperature distributions during the external thermal shock within the RPV and thermal insulation. Finding correlation or combination of correlations for the convection heat transfer coefficient during the transient cooling proved to be extremely challenging. A good agreement was found with combination of Chen correlation and correlation developed at Fortum for external post boiling. The validation of the script was done by using experimental and simulation data of the RPV without having any thermal insulation. Because of this the developed script performed well when any calculations were done by having one-layered system.

The developed script was slightly adjusted to include thermal insulation. The two-layered, thermally insulated system relies heavily on the assumption that the contact interface temperature between two different materials is infinitely close. Steady state calculations with thermally insulated system provided good consensus. Table 10 includes temperature distributions for the RPV with and without the thermal insulation for final comparison. Further development of the script would likely require experimental data. The estimated temperature distributions can be used as input data for stress calculations in part of RPV integrity assessment.

Table 10. Calculated temperatures at 5mm from the RPV surface to inwards (x=144mm).

Material/Time	5s	10s	15s	20s	25s	30s	40s
RPV	161.0	144.4	136.6	131.9	128.6	126.2	121.7
5mm thickness							
Macor	265.2	261.9	258.3	255.2	252.5	250.2	246.2
Calcium Silicate	266.0	265.4	264.5	263.5	262.6	261.7	260.2
AISI316	239.1	215.7	201.4	191.4	184.0	178.1	168.9
Ti-6Al-4V	254.8	241.2	231.5	224.0	217.8	212.6	204.1
Zirconium	227.1	204.2	190.8	181.6	174.8	169.4	160.8
1cm thickness							
Macor	266.0	265.9	265.3	264.4	263.3	262.1	259.6
Calcium Silicate	266.0	266.0	266.0	265.9	265.7	265.5	265.0
AISI316	260.3	245.5	233.0	223.4	215.6	209.2	198.9
Ti-6Al-4V	264.9	259.2	252.9	247.3	242.4	238.2	231.2
Zirconium	248.4	229.5	217.1	208.0	200.8	194.8	185.2
2cm thickness							
Macor	266.0	266.0	266.0	266.0	266.0	265.9	265.8
AISI316	265.9	264.2	260.2	255.3	250.2	245.3	236.4
Ti-6Al-4V	266.0	265.8	265.1	263.6	261.8	259.7	255.5
Zirconium	263.6	254.3	245.1	237.3	230.8	225.2	216.0

Further research on the subject is required. The heat transfer test facility in LUT (see section 4.5) could be used to research thermal insulation effect on the outer surface during transient cooling. Following could be researched at the test facility:

- Temperature distributions and heat transfer behavior with thermal insulation.
- Research and development for precise heat transfer correlation for the intense cooling.
- How insulation thickness influences heat transfer taking place on the edges of the insulation.
- The impact of contact resistance between RPV wall and thermal insulation.
- Thermal shock impact on very thin thermal insulation materials.
- Heat transfer experiments for structures that restrict or prevent the contact of water to the welded seam surface. (E.g. maze-like structures, steel-wools.)

Future research is also required particularly on the attachment and installation challenges

of the thermal insulation. The installation of thermal insulation is very challenging due to restricted access on the external side of the RPV in Loviisa. The attachment method should be considered thoroughly since the thermal insulation should stay intact during all accident scenarios.

REFERENCES

1. IAEA. Guidelines on Pressurized Thermal Shock Analysis for WWER Nuclear Power Plants. 2006. IAEA-EBP-WWER-08 (Rev. 1)
2. IAEA. Integrity of Reactor Pressure Vessels in Nuclear Power Plants: Assessment of Irradiation Embrittlement Effects in Reactor Pressure Vessel Steels. 2009. ISBN 978-92-0-101709-3.
3. United States Nuclear Regulatory Commission. Recommended Screening Limits for Pressurized Thermal Shock (PTS). 2010. NUREG-1874.
4. IAEA. Pressurized Thermal Shock in Nuclear Power Plants: Good Practices for Assessment. 2010. IAEA-TECDOC-1627.
5. Launiainen, S. Loviisa 1, PTS, Termohydrauliikkaketjujen valinta reaktoripainesäiliön deterministä turvallisuusanalyysia varten. Fortumin sisäinen dokumentti. 2011. ID: LO1-K311-001-00348.
6. APROS brochure. Retrieved 3.1.2017 from: http://www.apros.fi/filebank/213-Apros_Nuclear_brochure.pdf
7. Iyer, K., Nourbakhsh, H.P., & Theofanous, T.G. REMIX: a computer program for temperature transients due to high pressure injection after interruption of natural circulation. 1986. NUREG/CR--3701
8. Anon, Input Information For Qualification Of Inspection Object, RPV External Inspection. Fortum internal document. 2014. ID: LO1-K311-001-0088.
9. Lendell E. Steele. Radiation Embrittlement of Nuclear Reactor Pressure Vessel Steels: An International Review (Second Volume). 1986. ASTM (American Society for Testing and Materials). ISBN 0-8031-0473-1.
10. Neuvonen, A. Reaktoripainesäiliön PTS-lujuusanalyysien lähtötiedot. Fortumin sisäinen dokumentti. 2002. ID: NUCL-1302.
11. Kohopää, J. Reaktoripaineastian materiaalit. Fortumin sisäinen dokumentti. 2004. ID: LO1-K852-00499.
12. Launiainen, S. Loviisa 1, Reaktoripainesäiliön deterministinen haurasmurtuma-analyysi. Fortumin sisäinen dokumentti. 2011. ID: LO1-K311-001-00341.
13. Launiainen, S. Loviisa1 ja 2, PTS, Suojarakennuksen TQ-ruiskutuksen virheellinen käynnistyminen. Fortumin sisäinen dokumentti. 2011. ID: LO1-K311-001-00345.

14. Anon, Loviisa 1 Reaktoripainesäiliön deterministinen turvallisuusanalyysi. Fortumin sisäinen dokumentti. 2011. ID: LO1-K311-001-00343.
15. Incropera, F.P., Dewitt, D.P., Bergman, T.L., Lavine, A.S. Fundamentals of Heat and Mass Transfer. Sixth Edition, 2006. John Wiley & Sons.
16. Croy, D.E., Dougherty, D.A. Handbook of Thermal Insulation Applications, 1983. EMC ENGINEERS, INC.
17. Lahtinen, T. LO1 Reaktoripainesäiliön pinnoitteen neutroniannokset ja DPA-ekvivalentit neutroniannokset vuonna 2027. 2011. Fortumin sisäinen dokumentti. ID: LO1-K311-001-00332.
18. Einar Bardal. Corrosion and Protection. 2004. Springer. (94-107).
19. National Aeronautics and Space Administration. Nuclear and Space Radiation Effects on Materials. 1970. NASA SP-8053.
20. Macor brochure. Retrieved 19.8.2016 from: https://www.corning.com/media/worldwide/csm/documents/71759a443535431395eb34ebead091cb.pdf
21. Calcium Silicate brochure. Retrieved 3.9.2016 from: http://www.promat-hpi.com/downloads/get/en/8D778F21B04244AEA2A141C9F5E3DD46
22. AISI316 brochure. Retrieved 20.10.2016 from: http://www.aksteel.com/pdf/markets_products/stainless/austenitic/316_316l_data_sheet.pdf
23. Titanium brochure. Retrieved 24.10.2016 from: https://mdmetric.com/tech/ti6Al-4V.htm
24. Lamarsh, J.R., Baratta, A.J. Introduction to Nuclear Engineering. Third Edition. 2001. Prentice Hall.
25. Merisaari Timo. Heat Transfer Experiments for External Cooling of a Nuclear Reactor Pressure Vessel. 2008. Master's Thesis.
26. IAEA. Thermohydraulic relationships for advanced water cooled reactors. 2001. IAEA-TECDOC-1203.
27. Chen, J.C., A Correlation for Boiling Heat Transfer to Saturated Fluids in Convective Flow. 1966. Industrial and Engineering Chemistry, Process Design and Development.

28. Forster, H.K., Zuber, N., Dynamics of Vapor Bubbles and Boiling Heat Transfer. 1955. AIChE Journal, Vol. 1, (531-535)
29. Myllymäki, K. Lämmönsiirtokertoimen kokeellinen sovite paineastian ulkopuoliselle jäähdytykselle. Fortumin sisäinen dokumentti. 2008. ID: FNS-TERMO-125.
30. Taler, J., Duda, P. Solving Direct and Inverse Heat Conduction Problems. 2006. Springer.
31. FLUENT brochure. Retrieved 4.1.2017 from: http://resource.ansys.com/staticassets/ANSYS/staticassets/resourcelibrary/brochure/ansys-fluent-brochure-14.0.pdf